



SERVICE  
ALTIMÉTRIE  
&  
LOCALISATION  
PRÉCISE



CalVal

## Jason 3 validation and cross-calibration activities - (Annual Report 2016)

Reference: SALP-RP-MA-EA-23060

Nomenclature: -

Issue: 1. 2

Date: Mar. 29, 17

CLS (siège)  
8-10 rue Hermès  
Parc technologique du Canal  
31520 Ramonville Saint-Agne  
FRANCE

Tél. : +33 (0)5 61 39 47 00  
Fax : +33 (0)5 61 75 10 14  
Mél. : [info@cls.fr](mailto:info@cls.fr)  
Web : [www.cls.fr](http://www.cls.fr)

CLS Brest Le Ponant  
Avenue La Pérouse  
29280 Plouzané  
FRANCE

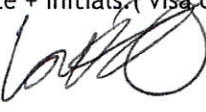

Tél. : +33 (0)2 98 05 76 80  
Fax : +33 (0)2 98 05 76 90



**Chronology Issues:**

Issue:	Date:	Reason for change:	Author
1.0	13/01/17	Creation	O. Lauret
1.1	24/03/17	Comments from NPicot.	O. Lauret
1.2	29/03/17	Minor changes	O. Lauret

**People involved in this issue:**

Written by (*):	O. Lauret S. Philipps M. Lievin	Date + Initials:( visa or ref) 
Checked by (*):	<i>Jp Oumant</i>	Date + Initial:( visa ou ref) <i>30-03-17</i> 
Approved by (*):		Date + Initial:( visa ou ref)
Application authorized by (*):		Date + Initial:( visa ou ref)

\*In the opposite box: Last and First name of the person + company if different from CLS

**Index Sheet:**

Context:	
Keywords:	[ Mots clés ]
Hyperlink:	



Distribution:		
CNES	electronic copy	thierry.guinle@cnes.fr emilie.bronner@cnes.fr jean-damien.desjonqueres@cnes.fr nicolas.picot@cnes.fr dominique.chermain@cnes.fr delphine.vergnoux@cnes.fr
Notification		



## List of tables and figures

### List of tables:

Table 1: List of GDR version "d" standard .....	3
Table 2: Events on Jason-3 mission .....	4
Table 3: List of missing Jason-3 passes.....	6

### List of figures:

Figure 1: Global GDRs data availability per cycle .....	5
Figure 2: Data availability over land for Jason 3 cycle 4(left) and Jason 2 cycle 284(right). ...	6
Figure 3: Jason-2 and Jason-3 GDR data availability over ocean (per cycle).....	7
Figure 4: Jason 3 daily data editing. The data gap in march is not due to data editing but to missing measurements (GPS platform upload). ....	8
Figure 5: (Top) Edited data based on the number of 20Hz measurements necessary to compute 1Hz measurement. (Bottom) Edited data based on the standard deviation of 20Hz measurements thresholds. ....	9
Figure 6: Percentage of data edited by SWH thresholds criteria and compared with Jason 2 on a cyclic basis.....	10
Figure 7: Percentage of data edited by Sigma 0 (top) and Standard deviation of Sigma 0 (bottom) thresholds criteria for Jason 3 and Jason 2 on a cyclic basis. ....	10
Figure 8: Percentage of data edited by radiometer wet tropospheric correction thresholds criteria for Jason 3 and Jason 2 on a cyclic basis. ....	11
Figure 9: Percentage of data edited by ionospheric correction thresholds criteria for Jason 3 and Jason 2 on a cyclic basis.....	11
Figure 10: Percentage of data edited following wind speed thresholds criteria for Jason 3 and Jason 2 on a cyclic basis. ....	12
Figure 11: Percentage of data edited by sea state bias thresholds criteria for Jason 3 and Jason 2 on a cyclic basis. ....	12
Figure 12: Percentage of data edited by ocean tide thresholds criteria for Jason 3 and Jason 2 on a cyclic basis.....	13
Figure 13: Percentage of data edited by mispointing thresholds criteria for Jason 3 and Jason 2 on a cyclic basis. ....	13
Figure 14: Percentage of data edited by sea surface heights thresholds criteria for Jason 3 and Jason 2 on a cyclic basis. ....	14
Figure 15: Percentage of data edited by sea level anomaly thresholds criteria for Jason 3 and Jason 2 on a cyclic basis. ....	14
Figure 16: Daily monitoring of number of elementary 20 Hz range measurements for Jason 3 and Jason 2 in Ku band.....	15
Figure 17: Mean of Jason 2-Jason 3 differences from cycle 0 to 22, Ku band. ....	16
Figure 18: Daily monitoring of 20 Hz range measurements standard deviation for Jason 3 and Jason 2 in Ku band. ....	16
Figure 19: Daily monitoring of number of elementary 20 hz range measurements for Jason 3 and Jason 2 in C band. ....	17



Figure 20: Daily monitoring of 20 Hz range measurements standard deviation for Jason 3 and Jason 2 in C band.....	17
Figure 21: Mean of Jason 2-Jason 3 differences from cycle 0 to 22, C band. ....	18
Figure 22: Daily monitoring of square of nadir angle for Jason 3 and Jason 2, IGDR mode.....	19
Figure 23: Daily monitoring of square of nadir angle for Jason 3 and Jason 2, GDR mode.....	19
Figure 24: Daily monitoring of Sigma 0 for Jason 3 and Jason 2 in Ku band. ....	20
Figure 25: Daily monitoring of Sigma 0 for Jason 2 and Jason 1 in Ku band. ....	20
Figure 26: Mean of Jason 2-Jason 3 differences from cycle 0 to 22, Ku band.....	21
Figure 27: Daily monitoring of Sigma 0 for Jason 3 and Jason 2 in C band.....	21
Figure 28: Mean of Jason 2-Jason 3 differences from cycle 0 to 22, C band. ....	22
Figure 29: Daily monitoring of Significant Wave Heights for Jason 3 and Jason 2 in Ku band..	22
Figure 30: Mean of Jason 2-Jason 3 differences from cycle 0 to 22, Ku band.....	23
Figure 31: Daily monitoring of Significant Wave Heights for Jason 3 and Jason 2 in C band. ..	23
Figure 32: Mean of Jason 2-Jason 3 differences from cycle 0 to 22, C band. ....	24
Figure 33: Daily monitoring of ionosphere correction for Jason 3 and Jason 2: in GDR mode (top) and in IGDR mode (bottom).....	25
Figure 34: Mean of Jason 2-Jason 3 differences from cycle 0 to 22. ....	25
Figure 35: Daily monitoring of wet tropospheric differences for Jason 3 and Jason 2, IGDR mode. ....	26
Figure 36: Daily monitoring of wet tropospheric correction for Jason 3 and Jason 2, GDR mode. ....	26
Figure 37: Daily monitoring of brightness temperatures and differences between Jason 3 and Jason 2, GDR mode.....	27
Figure 38: Mean of Jason 2-Jason 3 differences from cycle 0 to 22. ....	28
Figure 39: Mean of Jason 2-Jason 3 Tb differences (K) from cycle 0 to 22. ....	29
Figure 40: Daily monitoring of wind speed for Jason 3 and Jason 2. ....	30
Figure 41: Mean of Jason 2-Jason 3 differences from cycle 0 to 22. ....	30
Figure 42: Daily monitoring of sea state bias for Jason 3 and Jason 2. ....	31
Figure 43: Daily monitoring of sea state bias standard deviation for Jason 3 and Jason 2.....	31
Figure 44: Cyclic monitoring of crossover mean SSH differences for Jason 3 and Jason 2. ....	32
Figure 45: Map of crossover SSH differences Jason 3 vs Jason 3 for cycle 22. ....	33
Figure 46: Comparison of mean SSH crossover differences between OGDR and IGDR for Jason 3 and Jason 2 during the first 5 cycles. ....	34
Figure 47: Comparison of SSH standard deviation crossover differences between OGDR and IGDR for Jason 3 and Jason 2 during the first 5 cycles. ....	34
Figure 48: Map of crossover SSH differences Jason 3 vs Jason 2 from cycle 0 to cycle 22. ....	34
Figure 49: Cyclic monitoring of crossover mean SSH differences Jason 3 - Jason 2.....	35
Figure 50: Cyclic monitoring of crossover standard deviation SSH differences for Jason 3 and Jason 2.....	35
Figure 51: Mean of Jason 2-Jason 3 SLA differences cumulated over cycle 0 to 22.....	36
Figure 52: Mean of Jason 2-Jason 3 non corrected SLA (orbit - range - MSS) differences cumulated over cycle 0 to 22.....	36



Figure 53: Daily monitoring of mean SLA and differences between Jason 3 and Jason 2. ....	37
Figure 54: Daily monitoring of mean SLA and differences between Jason 3 and Jason 2. ....	37
Figure 55: Daily monitoring of mean SLA and differences between Jason 3 and Jason 2, IGDR mode. ....	38
Figure 56: T/P, JA1,JA2,JA3 concatenated after bias correction .....	39
Figure 57: Regional biases between Jason 3 and Jason 2 .....	40
Figure 58 : SLA spectra for Jason-2/Jason-3 and SARAL Altika from respectively 20 Hz and 40 Hz measurements .....	41
Figure 59 : Editing procedure adapted to high rate measurements for Jason-2/Jason-3 and SARAL/Altika missions .....	42
Figure 60 :: Map of SLA variance reduction applying new editing and Zaron's method (V1) compared to data processed with classical 1-Hz editing procedure (V0), after filtering out along-track data lower than 200 km. ....	43
Figure 61: SLA spectra applying new editing and Zaron's method (V1) compared to data processed with classical 1-Hz editing procedure (V0). ....	43



## List of Contents

<b>1. Introduction.....</b>	<b>1</b>
<b>2. Processing status.....</b>	<b>1</b>
2.1. Processing .....	1
2.2. List of events .....	3
<b>3. Data coverage and edited measurements .....</b>	<b>5</b>
3.1. Missing measurements .....	5
3.1.1. Over land and over ocean.....	5
3.1.2. Over ocean .....	6
3.2. Edited measurements .....	7
3.2.1. Global editing and thresholds .....	8
3.2.2. Threshold criteria: 20-Hz measurements number and standard deviation.....	9
3.2.3. Threshold criteria: Significant wave heights.....	9
3.2.4. Threshold criteria: Backscatter coefficient .....	10
3.2.5. Threshold criteria: Radiometer wet troposphere correction .....	10
3.2.6. Threshold criteria: Ionosphere correction .....	11
3.2.7. Threshold criteria: Wind speed.....	11
3.2.8. Sea State Bias.....	12
3.2.9. Ocean tide.....	12
3.2.10. Square of nadir angle .....	13
3.2.11. Sea surface heights .....	13
3.2.12. Sea level anomalies.....	14
<b>4. Monitoring of altimeter and radiometer parameters.....</b>	<b>15</b>
4.1. 20Hz measurements.....	15
4.2. Off Nadir Angle from waveforms .....	18
4.3. Backscatter coefficient .....	19
4.4. Significant Wave Heights .....	22
4.5. Dual frequency ionosphere correction .....	24
4.6. AMR Wet troposphere correction.....	26
4.7. Wind speed .....	29
4.8. Sea state bias .....	31
<b>5. Sea Surface Height crossover analysis.....</b>	<b>32</b>
5.1. Mean of SSH crossover differences.....	32
5.2. Mean of SSH crossover differences between Jason 3 and Jason 2 .....	34
5.3. Standard deviation of SSH crossover differences .....	35



<b>6. Sea Level Anomalies (SLA) along-track analysis .....</b>	<b>35</b>
<b>7. Mean Sea Level (MSL) calculation .....</b>	<b>39</b>
<b>8. Investigations .....</b>	<b>40</b>
<b>8.1. Altimetry errors for submesoscale .....</b>	<b>40</b>
8.1.1. Error description.....	40
8.1.2. Expected Improvements .....	41
<b>9. Conclusion.....</b>	<b>44</b>
<b>10. References.....</b>	<b>45</b>





## 1. Introduction

This document presents the synthesis report concerning validation activities of Jason-3 Geophysical Data Records (GDRs) under SALP contract (N° 160182/Lot 1.6.3) supported by CNES at the CLS Space Oceanography Division. This encompasses several points: CAL/VAL Jason-3 activities, Jason-3 / Jason-2 cross-calibration, particular studies and investigations.

Jason-3 satellite was successfully launched on January, 17th 2016. Since February, 12th, Jason-3 is on its operational orbit to continue the long term climate data record on the primary Topex, Jason-1, and OSTM/Jason-2 ground track.

Until October 2<sup>nd</sup>, 2016, Jason-3 and Jason-2 were in formation flight, with only 80 seconds delay, before Jason-2 was moved to the same interleaved orbit that was used by Topex from 2002-2005 and Jason-1 from 2009-2012.

The present document assesses the Jason-3 data quality. During each cycle, missing measurements were monitored, spurious data were edited and relevant parameters derived from instrumental measurements and geophysical corrections were analysed.

The document also focuses on Jason-3/Jason-2 cross-calibration. During the formation flight (February, 12th to October 2<sup>nd</sup> 2016) both satellites were on the same ground track, which is a unique opportunity to precisely assess parameter discrepancies between both missions and detect geographically correlated biases, jumps or drifts. The SLA performances and consistency with Jason-2 are also described, and one chapter is dedicated to the behaviour of on board AMR radiometer during the first year of the mission.

## 2. Processing status

### 2.1. Processing

OGDR and IGDR products are publicly available since June 30<sup>th</sup> 2016. OGDRs were generated in version "T" until cycle 18/pass 137, and then turned in "d" version. The first OGDR "d" file is:

*JA3\_OPN\_2PdS018\_137\_20160809\_080914\_20160809\_100739.nc*

Concerning IGDRs, they turned from "T" to "d" version a few days before OGDRs on June 27<sup>th</sup> (cycle 14/pass 143). The first IGDR "d" file is:

*JA3\_IPN\_2PdP014\_043\_20160626\_233040\_20160627\_002653.nc*

GDR products were made publicly available in November 2016. They were initially produced in "T" version until cycle 22 and then turned to "d" version. Pay attention that GDR "T" product contents and GDR "d" product content is identical for Jason-3.

The main differences between the O/IGDRs versions "T" and "d" are summarized hereafter:

- Cal-2 processing are based on typical ocean AGC values, correcting the negative squared-attitude values that were observed from the start of the mission.
- Backscatter (sigma-0) values are adjusted internally during ground processing. A calibration bias of +0.14 dB and +0.109 dB is added to the measured (and reported) MLE-4 and MLE-3 Ku-band sigma-0, respectively, prior to wind speed computation; a calibration bias of -0.231 dB and -0.012 dB is added to the measured (and reported) MLE-3 Ku- and C-band sigma-0, respectively, prior to rain flag computation and rain flag values. This ensure that they are properly aligned with the adopted algorithms, so that rain flagging and wind speed values are in-line with those from Jason-2.



The standards used for version “d” are listed in Table 1.

Model	Product Version “T”
Orbit	Based on Doris onboard navigator solution for OGDRs, DORIS tracking data for IGDRs (orbit standard “GRD-E”). DORIS and/or GPS tracking data for GDRs (orbit standard “GRD-E”).
Altimeter Retracking	<p><u>“OceanMLE4” retracking</u> MLE4 fit from 2<sup>nd</sup> order Brown analytical model : MLE4 simultaneously retrieves the 4 parameters that can be inverted from the altimeter waveforms:</p> <ul style="list-style-type: none"> <li>- Epoch (tracker range offset) <math>\Rightarrow</math> altimeter range</li> <li>- Composite Sigma <math>\Rightarrow</math> SWH</li> <li>- Amplitude <math>\Rightarrow</math> Sigma0</li> <li>- Square of mispointing angle (Ku band only, a null value is used in input of the C band retracking algorithm)</li> </ul> <p><u>“OceanMLE3” retracking</u> MLE3 fit from first order Brown analytical model: MLE3 simultaneously retrieves the 3 parameters that can be inverted from the altimeter waveforms:</p> <ul style="list-style-type: none"> <li>- Epoch (tracker range offset) <math>\Rightarrow</math> altimeter range</li> <li>- Composite Sigma <math>\Rightarrow</math> SWH</li> <li>- Amplitude <math>\Rightarrow</math> Sigma0</li> </ul> <p><u>“Ice” retracking</u> Geometrical analysis of the altimeter waveforms, which retrieves the following parameters:</p> <ul style="list-style-type: none"> <li>- Epoch (tracker range offset) <math>\Rightarrow</math> altimeter range</li> <li>- Amplitude <math>\Rightarrow</math> Sigma0</li> </ul>
Altimeter Instrument Corrections	Two sets: <ul style="list-style-type: none"> <li>- one set consistent with MLE4 retracking</li> <li>- one set consistent with MLE3 retracking</li> </ul>
Jason-3 Advanced Microwave	Using parameters derived from long term calibration tool developed and operated by NASA/JPL
Dry Troposphere Range Correction	From ECMWF atmospheric pressures and model for S1 and S2 atmospheric tides
Wet Troposphere Range Correction from Model	From ECMWF model
Ionosphere correction	Based on Global Ionosphere TEC Maps from JPL



Sea State Bias	Two empirical models: - MLE4 version derived from 1 year of MLE4 Jason-2 altimeter data with version "d" geophysical models - MLE3 version derived from 1 year of MLE3 Jason-2 altimeter data with version "d" geophysical models
Mean Sea Surface	MSS_CNES-CLS11
Mean Dynamic Topography	MDT_CNES-CLS09
Geoid	EGM96
Bathymetry Model	DTM2000.1
Inverse Barometer Correction	Computed from ECMWF atmospheric pressures after removing S1 and S2 atmospheric tides
Non-tidal High-frequency Dealiasing Correction	Mog2D High Resolution ocean model on (I)GDRs. None for OGDs. Ocean model forced by ECMWF atmospheric pressures after removing S1 and S2 atmospheric tides
Tide Solution 1	GOT4.8 + S1 ocean tide. S1 load tide ignored
Tide Solution 2	FES2004 + S1 and M4 ocean tides. S1 and M4 load tides
Equilibrium long-period ocean tide model	From Cartwright and Taylor tidal potential
Non-equilibrium long-period	Mm, Mf, Mtm, and Msqm from FES2004
Solid Earth Tide Model	From Cartwright and Taylor tidal potential
Pole Tide Model	Equilibrium model
Wind Speed from Model	ECMWF model
Rain Flag	Derived from comparisons to thresholds of the radiometer-derived integrated liquid water content and of the difference between the measured and the expected Ku-band backscatter coefficient
Ice Flag	Derived from comparison of the model wet tropospheric correction to a dual-frequency wet tropospheric correction retrieved from radiometer brightness temperatures, with a default value issued from a climatology table

Table 1: List of GDR version "d" standard

## 2.2. List of events

The following table lists mostly planned events for the Jason-3 mission.

Start time	End time	Cycle	Event
15/02/2016 08:00:00	15/02/2016 18:04:28	0	Data gap due to first calibration in DIODE + MNT mode
16/02/2016 16:07:00	16/02/2016 16:38:59	0	POS3B instrument calibration
17/02/2016 11:21:37	17/02/2016 15:11:47	1	Cross manoeuvre of $\pm 0.3^\circ$ in roll and pitch.
08/03/2016 20:00:00	09/03/2016 00:00:01	3	Gyro calibration inducing strong platform mispointing.



11/03/2016 05:14:00	11/03/2016 05:34:00	3	AMR calibration maneuver inducing strong mispointing
15/03/2016	17/03/2016	3	Platform GPS upload, no data product available.
25/03/2016 09:30:15		4	Data gap due to AMR OFF / ON: around 2 minutes of radiometer values set to DV in the Mediterranean Sea.
06/04/2016 06:05:00	06/04/2016 06:36:59	5	POS3B calibration. Data gap on pass 235, that mainly concerns land data acquisition and a portion of Red Sea.
27/04/2016 11:38:21	27/04/2016 12:05:55	8	Data gap (duration : 00:27:34) on pass 17 due to OPS error
02/05/2016 14:34:23	02/05/2016 14:37:28	8	Data gap due to DEM patch upload.
07/07/2016 15:04:44	07/07/2016 15:11:15	15	Data gap on pass 061 due to AMR internal error
12/07/2016 04:30:48		15	Data gap on pass 178 due to AMR calibration maneuver, only land data are concerned.
07/11/2016 22:25:00		27	AMR calibration maneuver
27/11/2016 06:15:00	27/11/2016 06:46:59	29	POS3B calibration

Table 2: Events on Jason-3 mission



### 3. Data coverage and edited measurements

The Jason 3 metrics provided in this chapters and in the following ones are based on a time period starting at cycle 0 (February 12<sup>th</sup>, 2016) and ending at cycle 22 (September 22<sup>nd</sup>, 2016). However, in many statistics data from cycle 0 were not included because there is only 5 days of available data.

#### 3.1. Missing measurements

##### 3.1.1. Over land and over ocean

Jason-3 can use two on board tracking modes: Diode/DEM and median tracker. Median tracker was used from cycle 0 over land, and until cycle 6 over ocean; DEM mode was activated over ocean from cycle 6, and over all referenced inland waters. For Jason 3 the data coverage over land surface can be slightly different regarding to Jason 2 (Figure 2).

Figure 1 shows the percentage of available measurements for Jason-3 and Jason-2 for all kind of surfaces observed, computed with respect to a theoretical possible number of measurements. In average Jason 3 provides 95.62% of measurements over 22 cycles.

If data availability is excellent both for Jason 3 and Jason 2, there are two cycles where the results are different:

- For cycle 0 (February 12<sup>th</sup> to February 17<sup>th</sup>, 2016): Jason 3 cycle 0 is the first one on the same Jason 2 orbit, and has only 5 days - not 10 days as usual for one cycle. Thus for Jason 3 only half of measurements at most can be available.
- For cycle 3 GPS platform upload interrupted the data product generation for two days, which explains the lower data availability observed during this cycle.

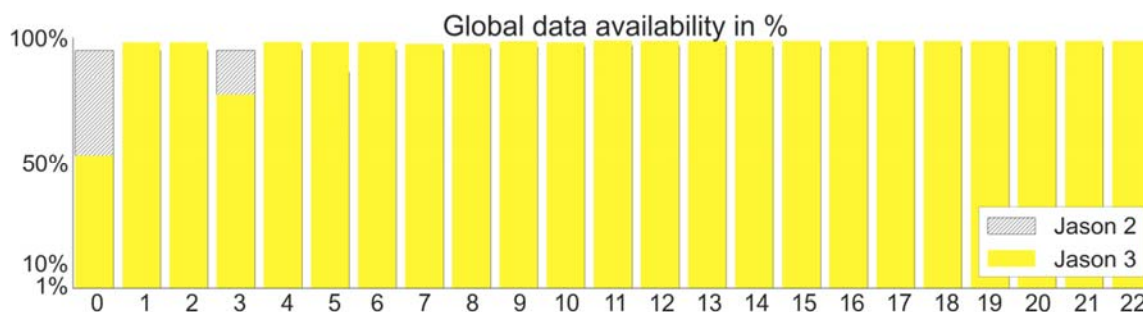


Figure 1: Global GDRs data availability per cycle

Concerning the data availability over land, it seems there are potentially more data available over land for Jason 3 than for Jason 2, even only median tracker is used and not DEM one. This difference is probably due to a limitation imposed on Jason 2 tracking to avoid ghost echoes.

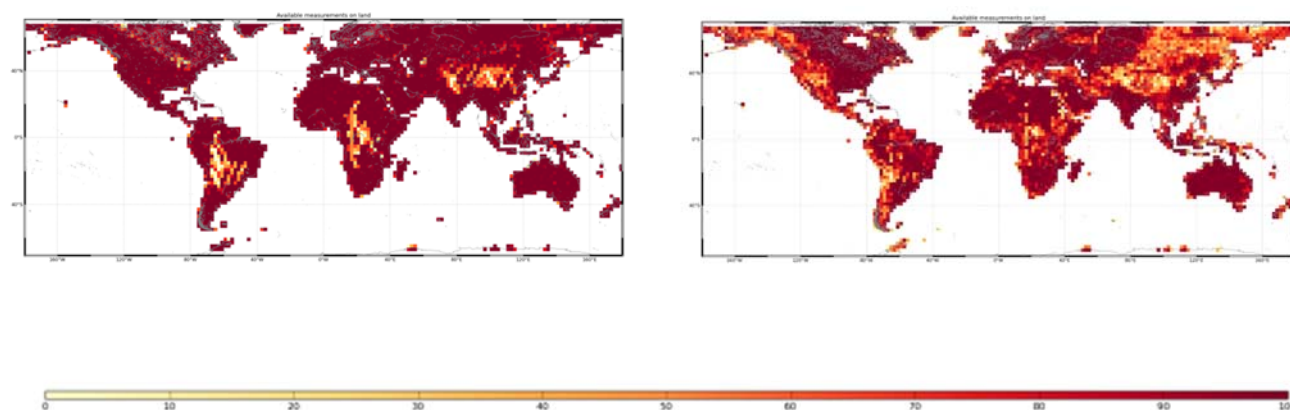


Figure 2: Data availability over land for Jason 3 cycle 4(left) and Jason 2 cycle 284(right).

Table 3 gives an overview of the missing passes (and the reason) for Jason-3

Jason-3 Cycle/Pass	Date	Reason
0/ 001 - 116	Before 12-02-2016 01:11:09	Final ground-track only reached on 12-02-2016 01:11:09
0/ 201, 203, 236		passes 201 (~10%), pass 203 (~12%) and pass 236 (~8%) partly missing due to calibration events
3/ 181 - 233	15-03-2016 07:15:04 to 17-03-2016 08:06:13	Due to platform GPS software upload, passes 182 to 232 are entirely missing, as well as part of passes 181 and 233.

Table 3: List of missing Jason-3 passes

### 3.1.2. Over ocean

Looking at data over ocean (figure 3), Jason 2 presents 95.60% of available measurements over the 22 cycles whereas Jason 3 has 97.36% of available measurements. Jason 2 had 9.66% of missing measurement during cycle 285 (cycle 5) due to GPS upload and AMR anomaly. Concerning Jason 3 there is 21.02% of missing measurements due to GPS platform upload during cycle 3, and cycle 0 is only half-a-cycle. Without taking into account such a specific event or big anomalies, Jason 3 available measurements are close to 99.97 %.

During this time period, the behaviour of Jason 3 over ocean is excellent and conform to what is observed with Jason 2 on the same ground track, with 80 seconds of difference.

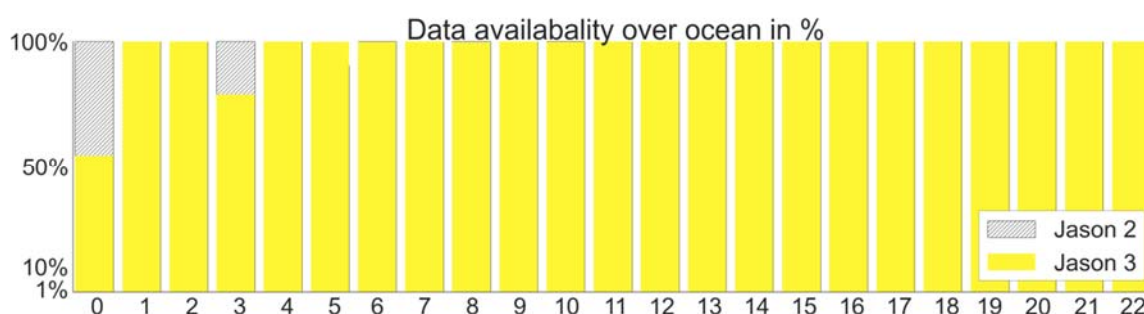


Figure 3: Jason-2 and Jason-3 GDR data availability over ocean (per cycle)

### 3.2. Edited measurements

Editing criteria allow to select only measurements considered as “valid” over ocean. This editing process is structured in 3 main steps.

1. First, measurements over land and over ice are removed.
2. Then, threshold criteria are applied on altimeter, radiometer and geophysical parameters and are described in the following table. Except for the dual frequency ionosphere correction, only Ku-band measurements are used in this editing procedure, as they mainly represent the end user dataset.
3. Moreover, a spline criterion is applied to remove the remaining spurious data.

For each criterion, the cycle per cycle percentage of edited measurements is monitored. This allows detection of anomalies in the number of removed data, which could have some instrumental, geophysical or algorithmic origins.

Tableau 1: Threshold editing criteria, Jason 3 and Jason 2

Parameter	Thrs Min	Thrs Max
LOW FREQ FLUCTUATIONS CORRECTION (ECMWF GAUSSIAN)	-2	2
DRY TROPOSPHERIC CORRECTION (ECMWF GAUSSIAN)	-2.5	-1.9
IONOSPHERIC CORRECTION	-0.4	0.04
IONOSPHERIC CORRECTION (GIM)	-0.4	0.04
OCEAN TIDE (GOT4V8)	-5	5
OCEAN TIDE EQ LONG PERIOD	-0.5	0.5
POLE TIDE HEIGHT MODEL (WAHR 85)	-15	15
RANGE NUMBER ALTI	10	20
RANGE STANDARD DEVIATION	0	0.2
NON PARAMETRIC SEA STATE BIAS	-0.5	0
ORBIT - RANGE	-130	100
SIGMA0 (*)	7 - -2.38	30 - -2.38
SIGMA0 NUMBER	10	20
SIGMA0 STANDARD DEVIATION	0	1





SEA SURFACE HEIGHT	-10	+ 10
- NON PARAMETRIC SEA STATE BIAS		
- SOLID EARTH TIDE (CARTWRIGHT TAYLER 71)		
- POLE TIDE (WAHR 85)		
- DYNAMICAL ATMOSPHERIC CORRECTION MOG2D HR		
- DRY TROPOSPHERIC CORRECTION (ECMWF GAUSSIAN)		
- OCEAN TIDE MODEL (GOT4V8)		
- WET TROPOSPHERIC CORRECTION		
- IONOSPHERIC CORRECTION		
- MEAN SEA SURFACE		
SOLID EARTH TIDE (CARTWRIGHT TAYLER 71)	-1	1
SQUARE OFF NADIR ANGLE	-0.2	0.64
SWH	0	11
WET TROPOSPHERIC CORRECTION	-0.5	-0.001
WIND SPEED	0	30

(\*) -2.38 dB is retired to be in agreement with TOPEX thresholds.

### 3.2.1. Global editing and thresholds

The percentage of total edited measurements is monitored on a daily basis. The average of total edited measurements is 37.75%, where 3.24% of data are edited following threshold criteria (see figure 4). The resulting difference between the two figures is due to data removed because of land or ice presence.

The total percentage is a little lower during March/April/May (30-35%), then increasing during May to July and remains around 38-42%, and start to slowly decrease in mid-September. This expected behaviour is related to sea ice coverage, and was already observed on previous altimetry missions such as OSTM/Jason 2.

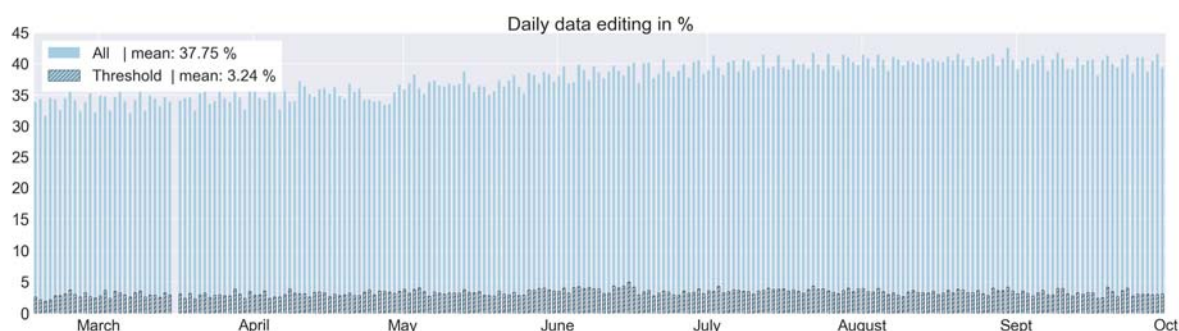


**Figure 4: Jason 3 daily data editing. The data gap in march is not due to data editing but to missing measurements (GPS platform upload).**

On the following figures please note that editing using threshold criteria is represented from cycle 1 to 22: cycle 0 is not took into account because containing half of data per cycle only.





### 3.2.2. Threshold criteria: 20-Hz measurements number and standard deviation

Measurements where less than 10 full resolution (20Hz, 20 measurements/seconds) measurements are available to compute 1Hz resolution range are removed. Such situations usually happen in regions with disturbed sea state or heavy rain. For Jason 3 the average percentage of removed measurements to compute altimeter range is 1.03% whereas it is 1.05% for Jason 2. The two missions provide very closed values.

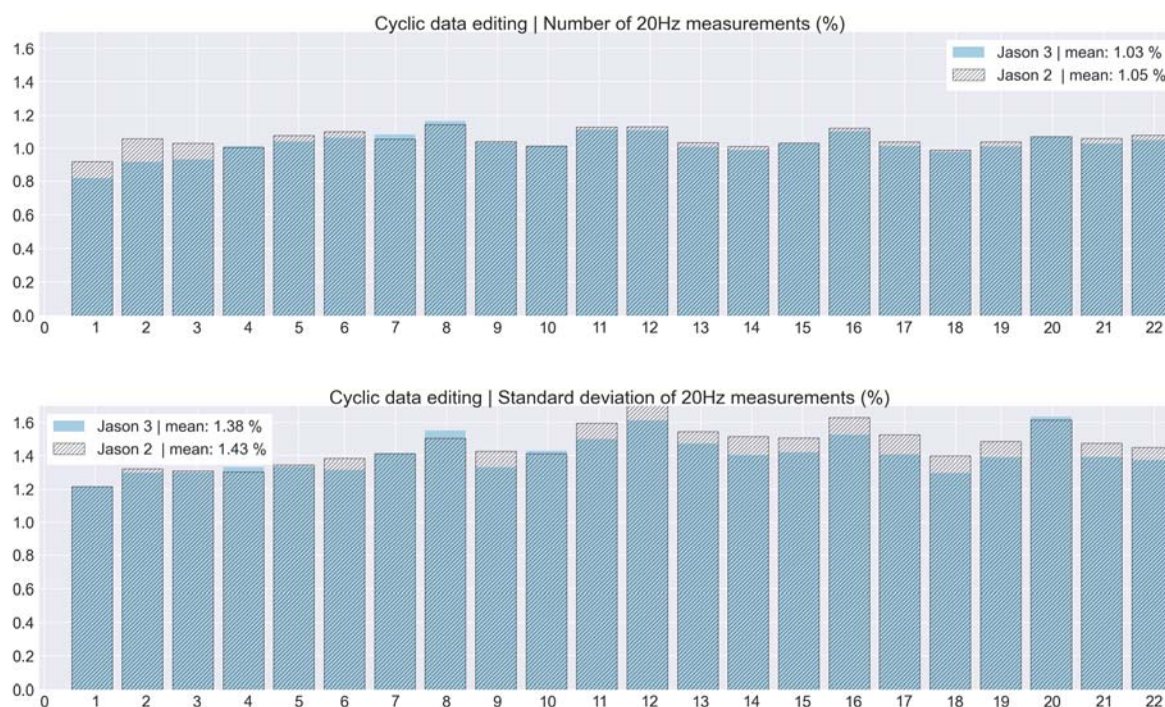


**Figure 5: (Top) Edited data based on the number of 20Hz measurements necessary to compute 1Hz measurement. (Bottom) Edited data based on the standard deviation of 20Hz measurements thresholds.**

With the threshold editing on the standard deviation for 20Hz measurements, 1.38% of data are removed in average. Note that it is expected to observe some annual signals here, but the time period for the analysis is too short (~7 months).

### 3.2.3. Threshold criteria: Significant wave heights

The percentage of edited measurements due to significant wave heights criterion is represented on figure 6, and is about 0.6%. They are mostly located near coasts in the equatorial regions and in circumpolar areas. Compared to Jason 2, it seems that the former remove more SWH data (0.65%).

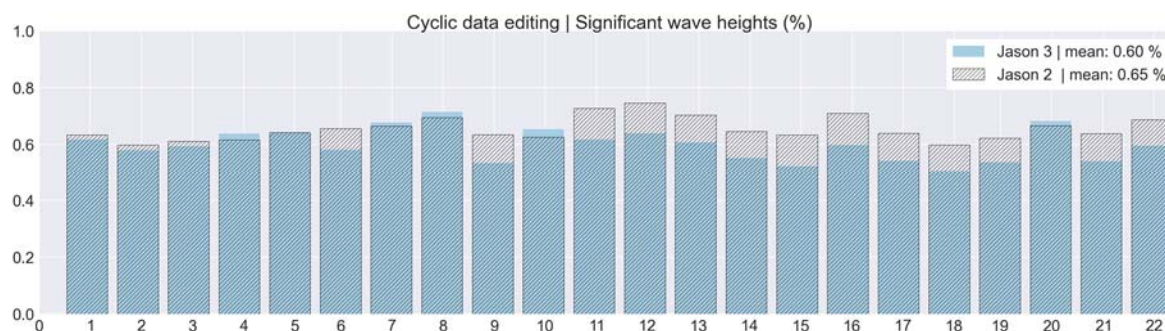


**Figure 6: Percentage of data edited by SWH thresholds criteria and compared with Jason 2 on a cyclic basis.**

### 3.2.4. Threshold criteria: Backscatter coefficient

The percentage of edited measurements due to backscatter coefficient criterion is represented in figure 7. It is about 0.55%, compared to 0.59% for Jason-2. The criteria based on standard deviation of Sigma 0 present again very close values between the two missions

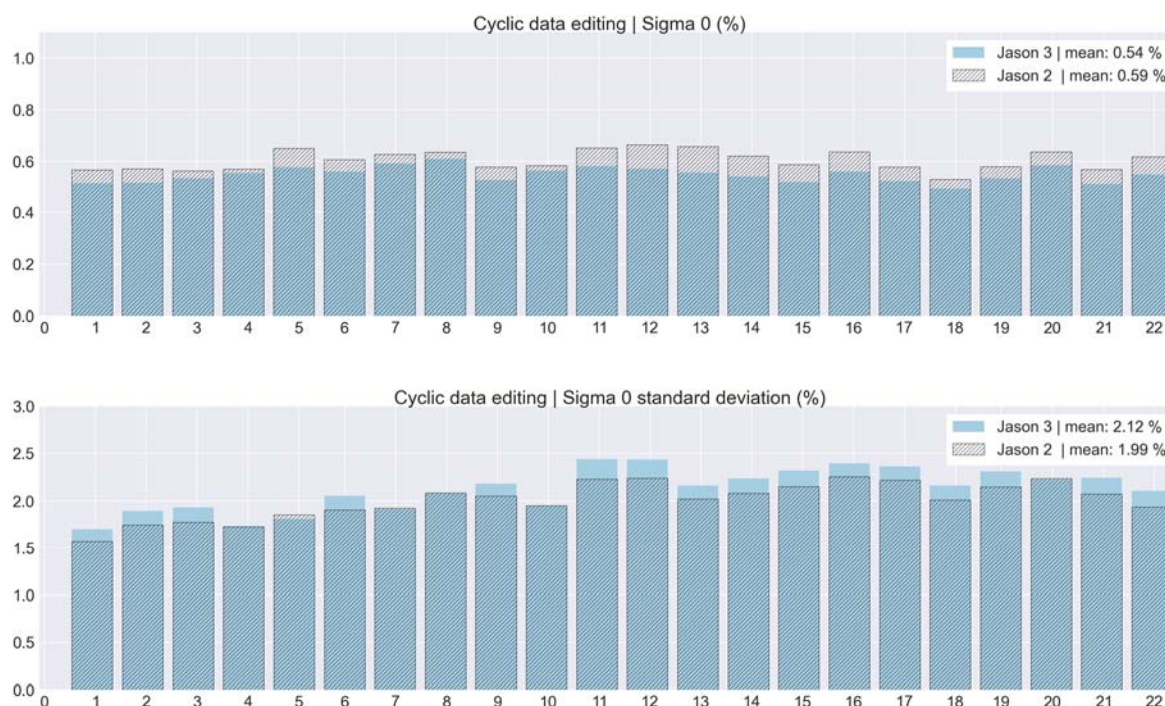


**Figure 7: Percentage of data edited by Sigma 0 (top) and Standard deviation of Sigma 0 (bottom) thresholds criteria for Jason 3 and Jason 2 on a cyclic basis.**

### 3.2.5. Threshold criteria: Radiometer wet troposphere correction

The mean edited data per cycle based on wet tropospheric correction thresholds is 0.09%. Compared to Jason-2 values, they are within the same order of magnitude, except specific events or anomalies





like during Jason 2 cycle 285 (Jason 3 cycle 5 on the figure below) where radiometer data are missing due to AMR anomaly.

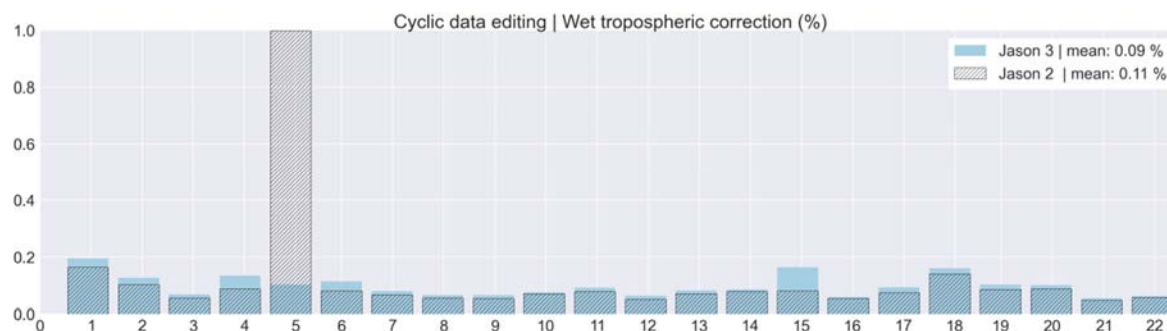


**Figure 8: Percentage of data edited by radiometer wet tropospheric correction thresholds criteria for Jason 3 and Jason 2 on a cyclic basis.**

### 3.2.6. Threshold criteria: Ionosphere correction

The mean percentage of edited data by threshold criteria on ionosphere correction is 1.16% and is very close to Jason 2 mean (1.19%).

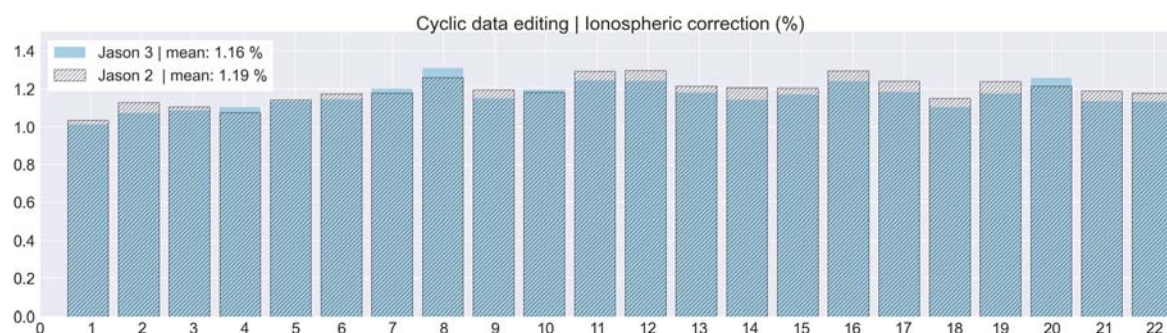


**Figure 9: Percentage of data edited by ionosphere correction thresholds criteria for Jason 3 and Jason 2 on a cyclic basis.**

### 3.2.7. Threshold criteria: Wind speed

The percentage of edited measurements due to altimeter wind speed criterion is about 1.07%, and is once again, very close to Jason 2 (1.02%). Measurements are usually edited because of default values. This is the case when sigma0 itself is at default value, or when it shows very high values (higher than 25 dB), which occurs during sigma bloom situations. Indeed, the wind speed algorithm based on sigma 0 and significant wave heights cannot retrieve values for sigma0 higher than 25 dB. Wind speed is also edited, when it has negative values - which can occur in GDR products. Nevertheless, sea state bias is available even for negative wind speed values.

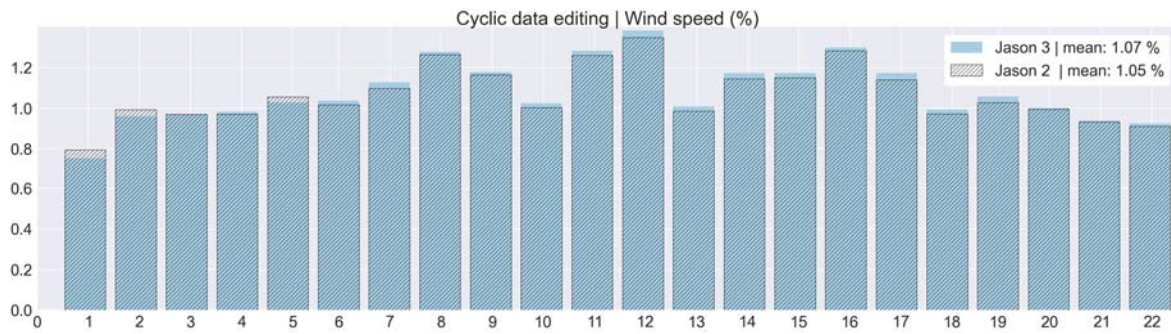


**Figure 10: Percentage of data edited following wind speed thresholds criteria for Jason 3 and Jason 2 on a cyclic basis.**

### 3.2.8. Sea State Bias

The percentage of Jason 3 edited measurements is about 0.51% and 0.63% for Jason 2, which underlines a slightly higher difference than usual between the two missions, slight difference that we can also observe on the sigma 0 (0.06%) and significant wave heights (0.05%) threshold criteria, which are at the origin of SSB computation.

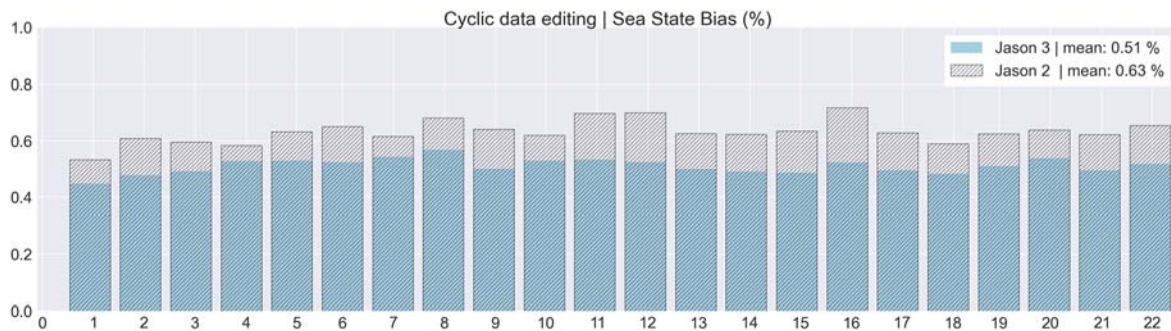


**Figure 11: Percentage of data edited by sea state bias thresholds criteria for Jason 3 and Jason 2 on a cyclic basis.**

### 3.2.9. Ocean tide

The percentage of edited measurements due to ocean tide is 0.01% for both missions. Basically they correspond to default values close to the coasts of Alaska or Labrador Sea.

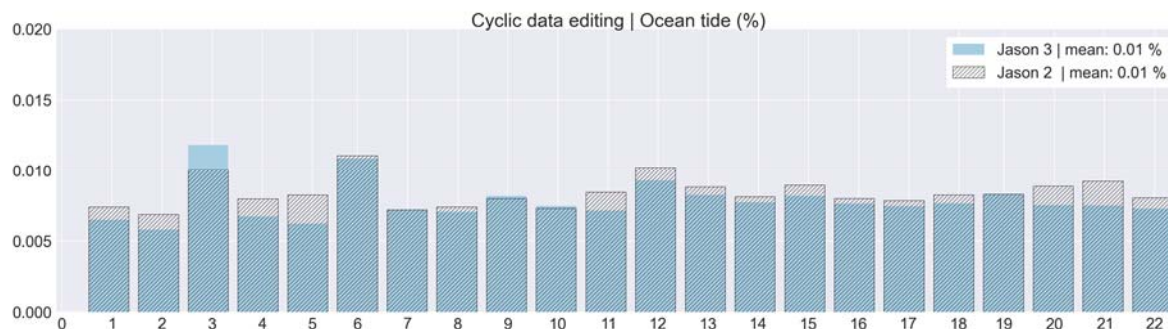


**Figure 12: Percentage of data edited by ocean tide thresholds criteria for Jason 3 and Jason 2 on a cyclic basis.**

### 3.2.10. Square of nadir angle

The percentage of edited data for both missions is similar (0.58%).

Most of edited data are default values due to sea state.

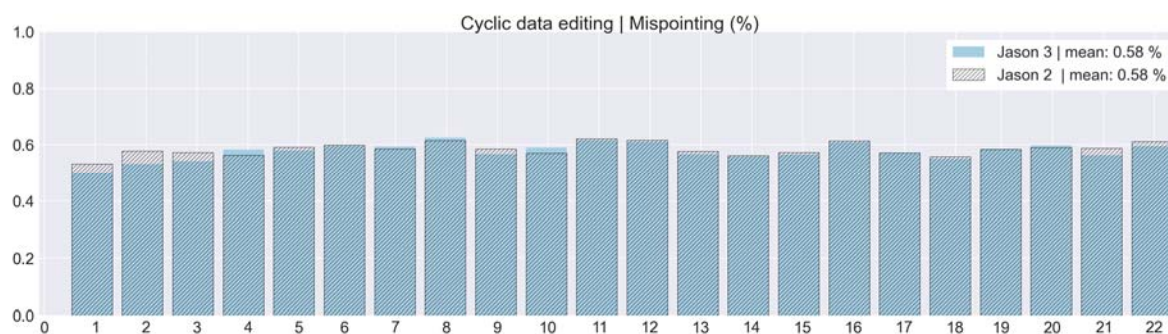


**Figure 13: Percentage of data edited by mispointing thresholds criteria for Jason 3 and Jason 2 on a cyclic basis.**

### 3.2.11. Sea surface heights

Sea surface heights represent the difference between the orbit and the altimeter range in Ku band.

The threshold criterion removes 0.75% of data for Jason 3 whereas it removes 0.77% for Jason 2. This is usually due to range measurements at default values near coast in equatorial and mid-latitude regions, as well as regions with low significant wave heights.



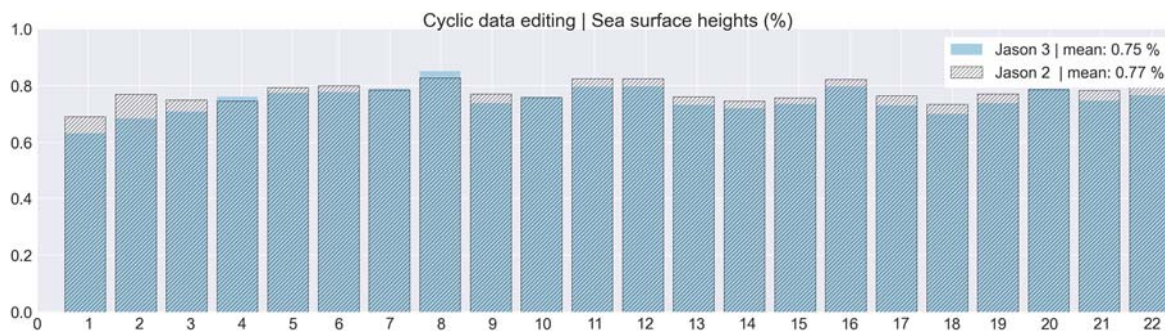


**Figure 14: Percentage of data edited by sea surface heights thresholds criteria for Jason 3 and Jason 2 on a cyclic basis.**

### 3.2.12. Sea level anomalies

The percentage of edited data by threshold criterion is 0.85% for Jason 3 and 1.04% for Jason 2; the difference is mainly due to Jason 2 wet troposphere contribution, where AMR was unavailable during cycle 285 (cycle 5 for Jason 3) leading to an increase of the quantity of edited data.

Otherwise the overall performance of the system is in excellent agreement between Jason 2 and Jason 3, and shows very close results in terms of edited data.

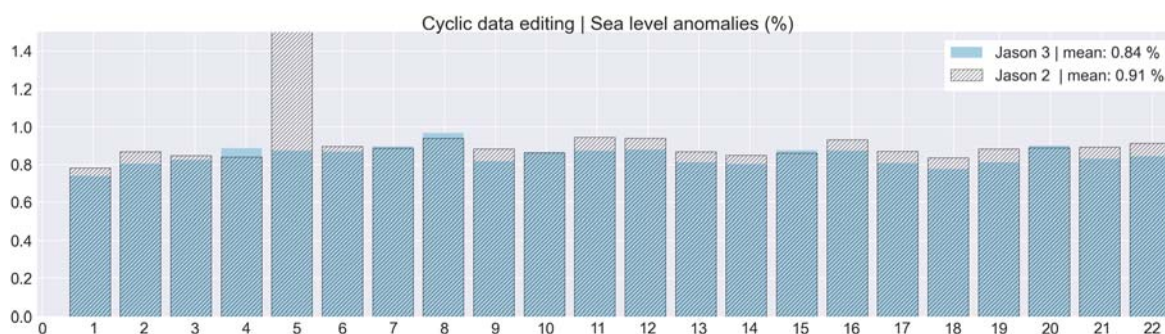


**Figure 15: Percentage of data edited by sea level anomaly thresholds criteria for Jason 3 and Jason 2 on a cyclic basis.**



## 4. Monitoring of altimeter and radiometer parameters

Both mean and standard deviation of the main parameters of Jason-3 were monitored since the beginning of the mission. Moreover, a comparison with Jason-2 parameters was also performed, that allows us to monitor the bias between the parameters of the 2 missions.

The monitoring period concerns formation flight where Jason 3 and Jason 2 are on the same ground track and spaced out about 80 seconds apart. Then the mean of the Jason 3 - Jason 2 differences can be computed using a point by point repeat track analysis.

### 4.1. 20Hz measurements

Number and standard deviation of 20 Hz elementary range measurements are computed during the altimeter ground processing. For both Jason-3 and Jason-2, before performing a regression to derive the 1 Hz range from 20 Hz data, a MQE (mean quadratic error) criterion is used to select valid 20 Hz measurements. This first step of selection consists in verifying that the 20 Hz waveforms can be approximated by a Brown echo model (Brown, 1977 [23]) (Thibaut et al. 2002 [61]).

Then, through an iterative regression process, elementary ranges that are too far from the regression line are discarded until convergence is reached. Thus, monitoring the number of 20 Hz range measurements and the standard deviation computed among them is likely to reveal changes at instrumental level.

Jason 3 number of elementary 20 Hz range measurements starts with values slightly higher than Jason 2 until cycle 3. During cycle 3 new CAL2 filter turned the square of nadir angle to zero, which means no waveform mispointing anymore, higher MQE and smaller number of elementary measurements. Then from cycle 4 onwards Jason 3 is very similar to Jason 2's (especially for Ku-band) with an average of 19.606 in Ku-band and 19.239 vs 19.255 in C-band (figures 16&19).

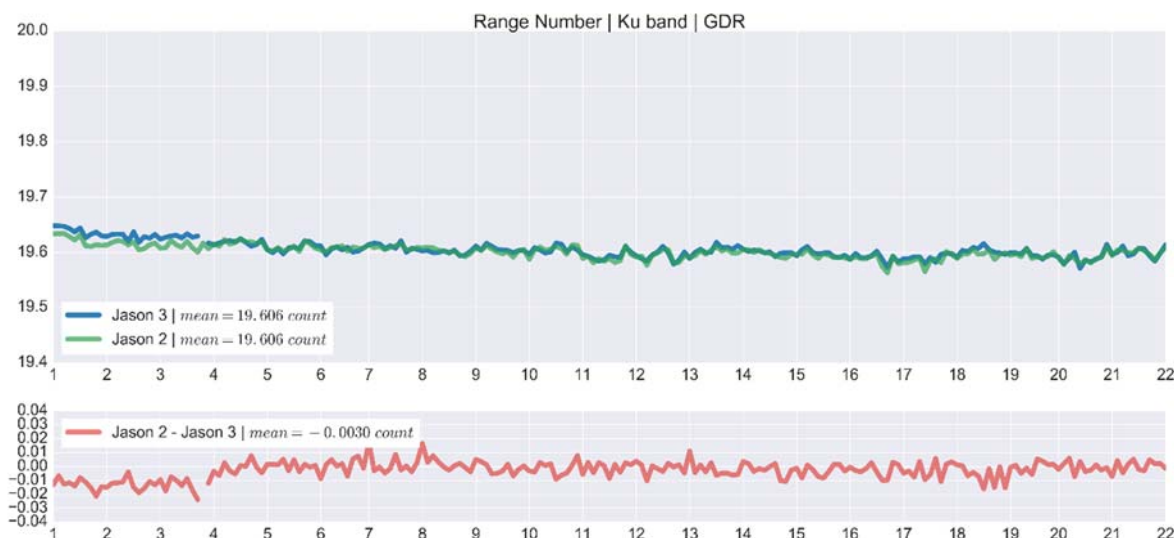


**Figure 16: Daily monitoring of number of elementary 20 Hz range measurements for Jason 3 and Jason 2 in Ku band.**

Differences between Jason 3 and Jason 2 in number of 20 Hz Ku-band is very close to zero.

The map of Jason 3 - Jason-2 differences display very small signals (difference of -0.0026 measurements between the missions).

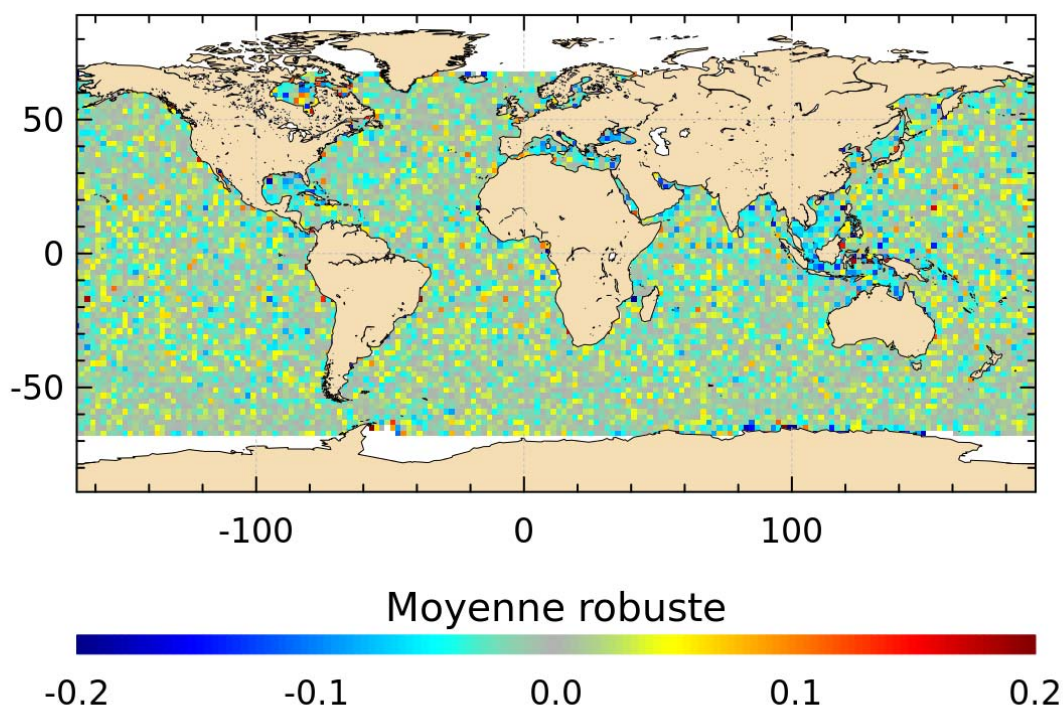


Figure 17: Robust mean of Jason 2-Jason 3 differences from cycle 0 to 22, Ku band.

Daily monitoring of 20 Hz range standard deviation is quite stable and does not display any anomaly. Jason-3 standard deviation of the 20 Hz measurements is 8.0 cm in Ku Band (Figure 18) and 17.7 cm in C Band (Figure 20). It is very similar to Jason-2 data, and no trend nor anomaly is observed.

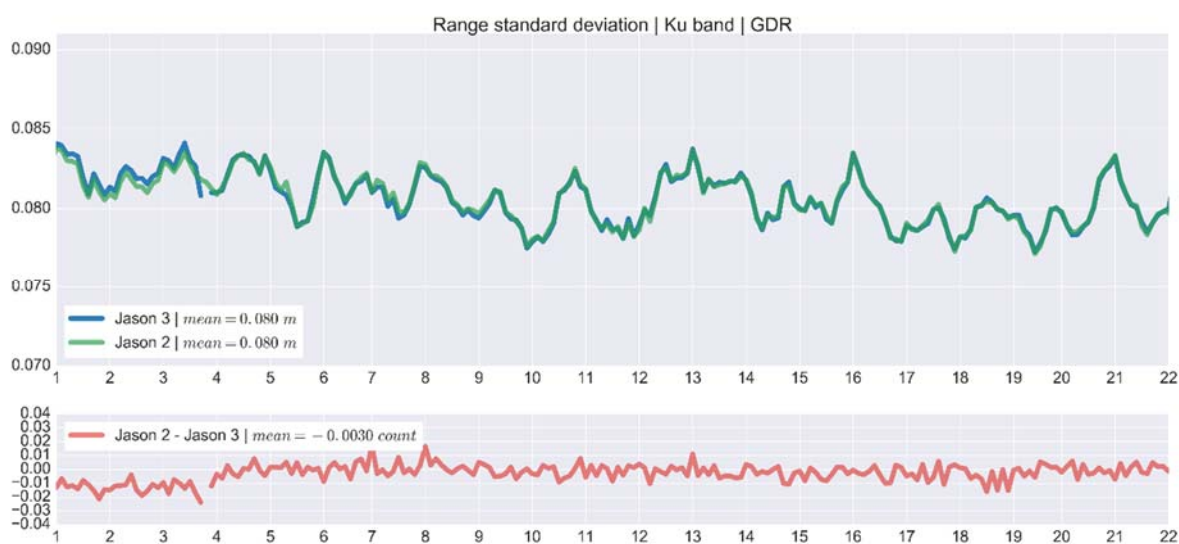


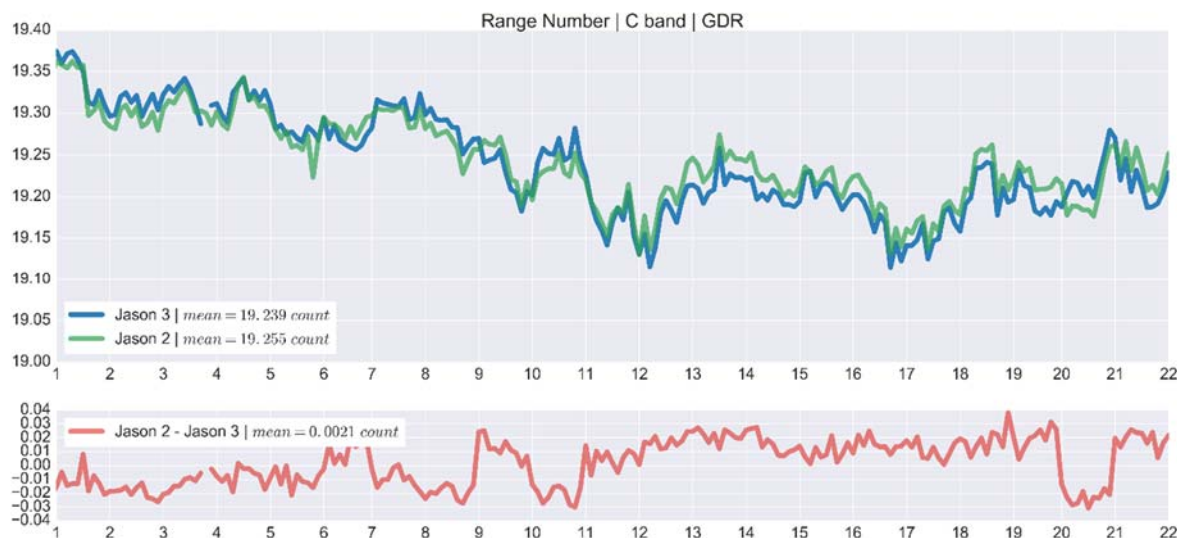
Figure 18: Daily monitoring of 20 Hz range measurements standard deviation for Jason 3 and Jason 2 in Ku band.

In C band Jason 3 number of 20Hz measurements is a little smaller than Jason 2's but still very close (19.239 vs 19.255, figure 19), and again very close in terms of standard deviation (figure 20). On

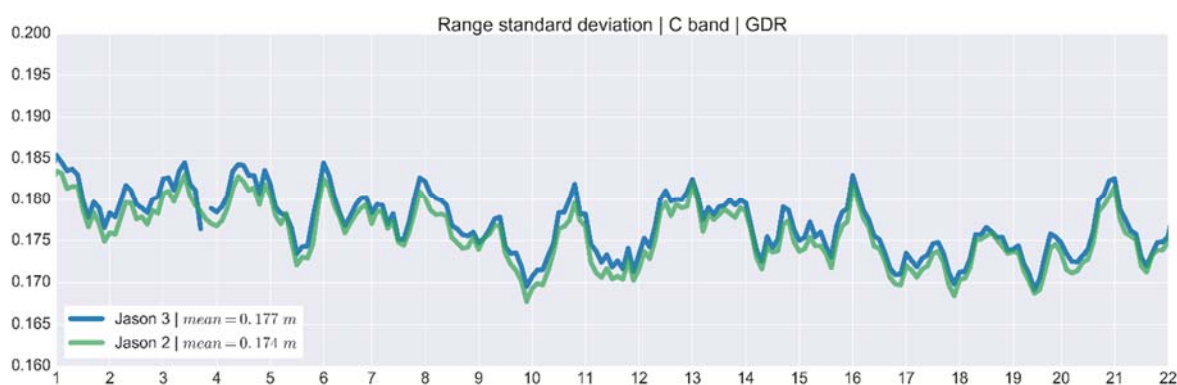




figure 19, before and after cycle 11 the parameter from both missions turns to a different behaviour (under investigation).



**Figure 19: Daily monitoring of number of elementary 20 Hz range measurements for Jason 3 and Jason 2 in C band.**



**Figure 20: Daily monitoring of 20 Hz range measurements standard deviation for Jason 3 and Jason 2 in C band.**

The map of differences in C band (figure 21) highlights Hudson Bay and Indonesia, a region where satellite altimetry is perturbed by sigma blooms and rain, which reduces the value of number of 20 Hz measurements to compute 1Hz data.

On the map the difference between both missions is positive, which means the number of 20 Hz measurements is a little higher for Jason 2; the small signatures observed in Hudson and Indonesia need further investigations.

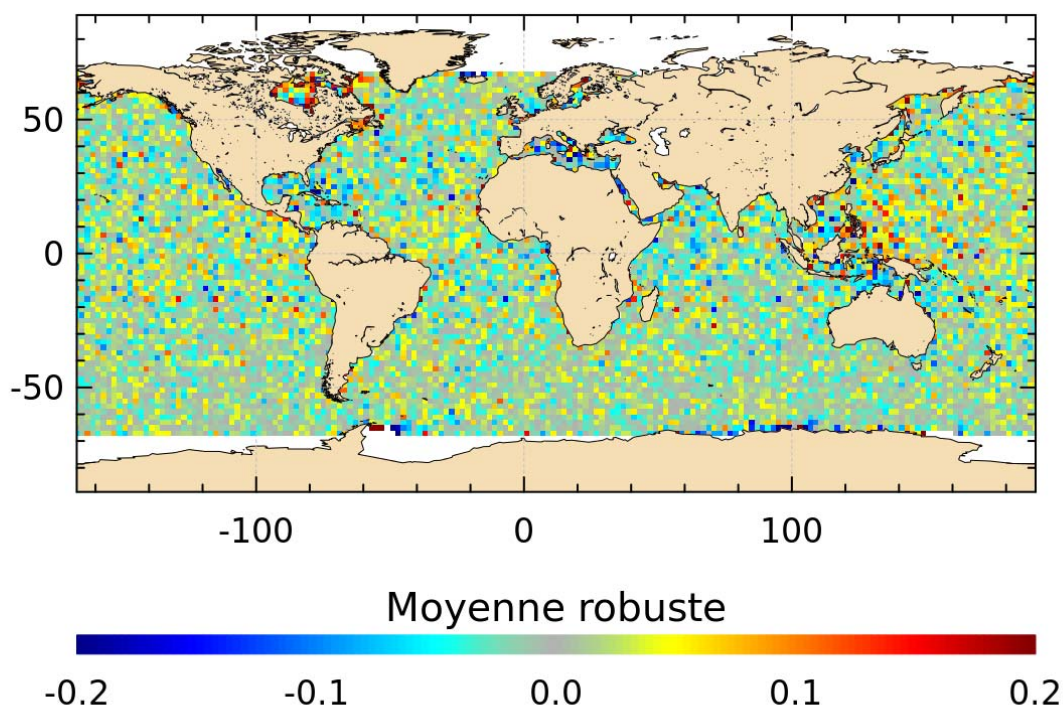


Figure 21: Robust Mean of Jason 2-Jason 3 differences from cycle 0 to 22, C band.

## 4.2. Off Nadir Angle from waveforms

The square of the off-nadir angle allows an estimation of Jason 3 mispointing; it is processed from the waveform shape during the altimeter retracking.

Jason-3 altimeter mispointing was deeply analysed to understand the negative values observed from cycle 3 after GPS upload (figure 22). Mispointing is actually related to CAL2 filter shapes, which depends on automatic gain control settings for Jason 3.

During the first cycles, the in-flight CAL2 filters were measured using a different Automatic Gain Control code than the one used during waveform acquisition over ocean, in order to optimize the CAL2 measurement numerical accuracy (quantification optimization). It has however an impact on the filter slope and fully explains the mispointing negative values observed.

The filter slope was modified during cycle 14 (June 26<sup>th</sup>, 2016, figure 22) and explains the “jump to zero” on the IGDR figure.

This correction was applied during GDR production, which explains the mispointing is close to zero from cycle 4 (figure 23).

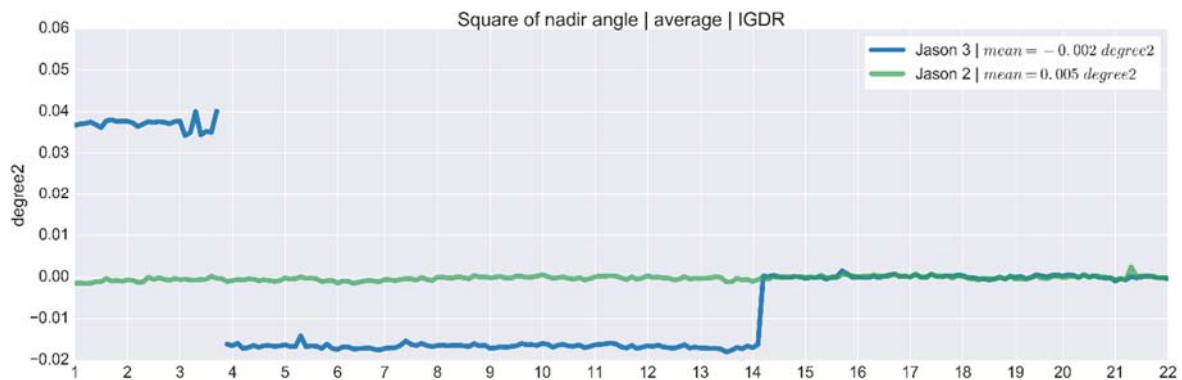


Figure 22: Daily monitoring of square of nadir angle for Jason 3 and Jason 2, IGDR mode.

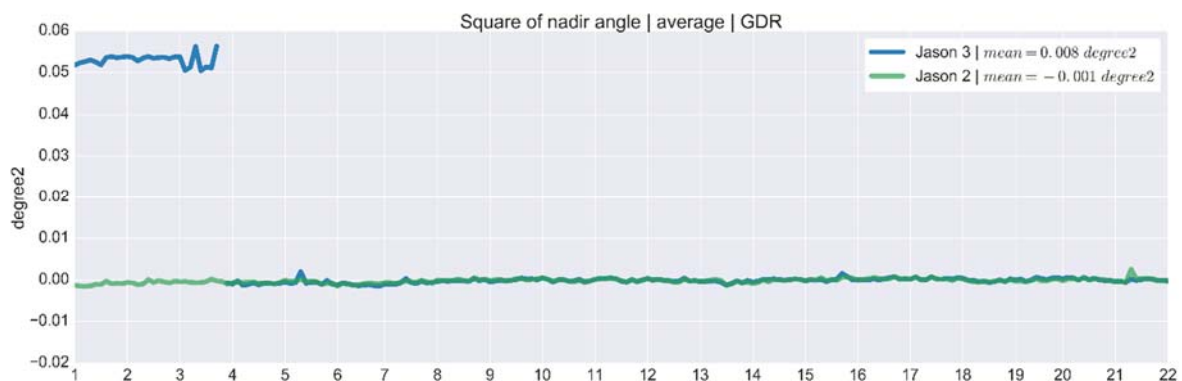


Figure 23: Daily monitoring of square of nadir angle for Jason 3 and Jason 2, GDR mode.

### 4.3. Backscatter coefficient

Jason-3 altimeter backscatter is in good agreement with Jason 2, both in Ku and C band, with respectively 13.75 dB and 13.54 dB in average. The difference between the two missions is about -0.25 dB and present a good stability (figure 24); however, this was different from cycle 0 to cycle 4, where slight mispointing on Jason 3 caused higher differences of  $\sigma_0$  between missions. We introduced as an example the same information computed during Jason 2 and Jason 1 formation flight (figure 25): this highlights the good stability of Jason 3/2  $\sigma_0$  regarding to Jason 2/1 where there are larger variations.

During formation flight Jason 3  $\sigma_0$  was modified with one new altimeter Characterization file, an update of the look up tables (Patch 6) and one new CAL2 filter (cycle 14, June 26<sup>th</sup>, 2016). All of them were applied on all GDR cycles.

From a geographic point of view there is a good consistency between JA2 and JA3  $\sigma_0$  in Ku band with small but significant residual signals ( $\pm 0.04$  dB); in C band, there is an unexpected “ground track” signal that is dominating (figures 26&28) (to be investigated).

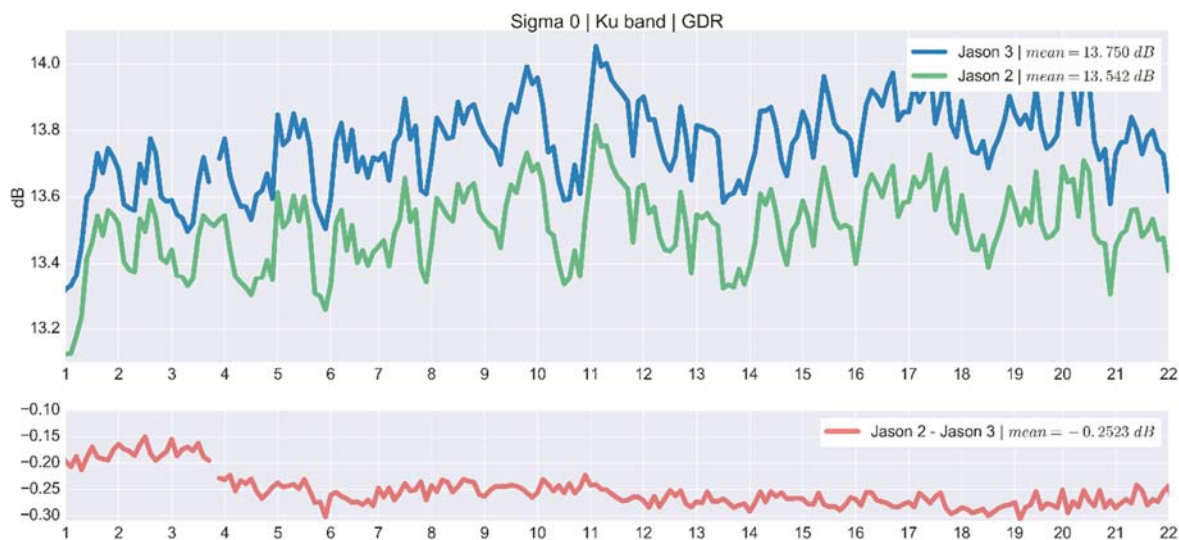


Figure 24: Daily monitoring of Sigma 0 for Jason 3 and Jason 2 in Ku band.

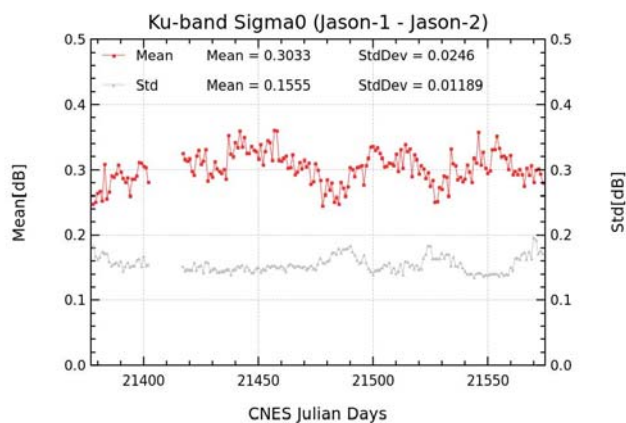


Figure 25: Daily monitoring of Sigma 0 for Jason 2 and Jason 1 in Ku band.



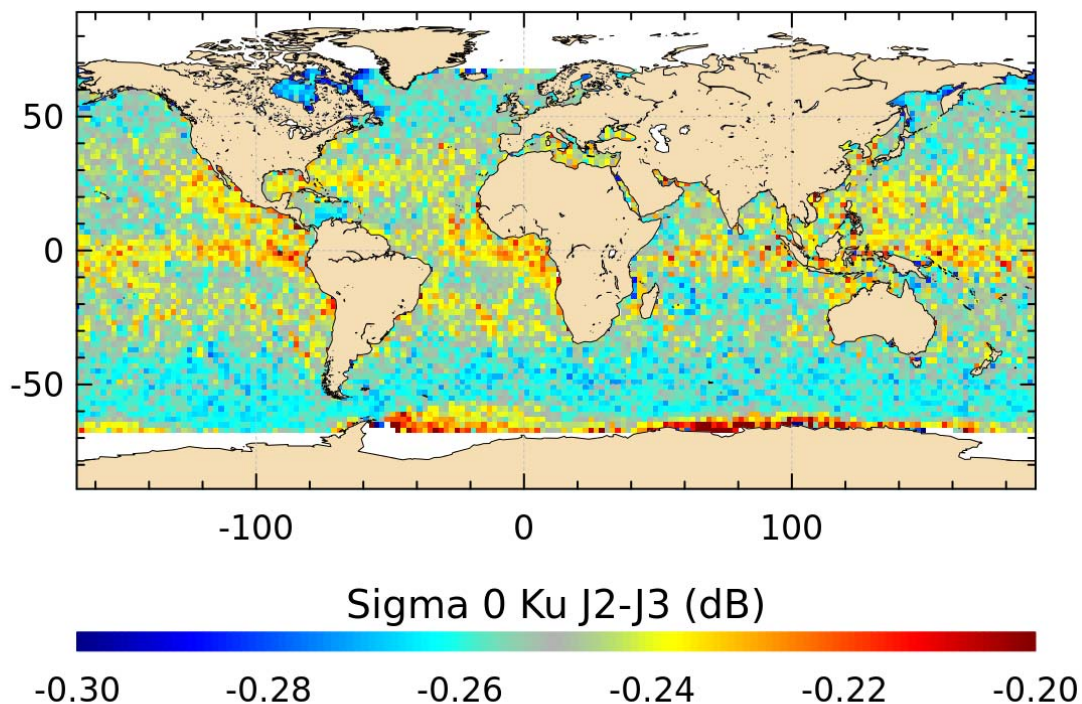


Figure 26: Mean of Jason 2-Jason 3 differences from cycle 0 to 22, Ku band.

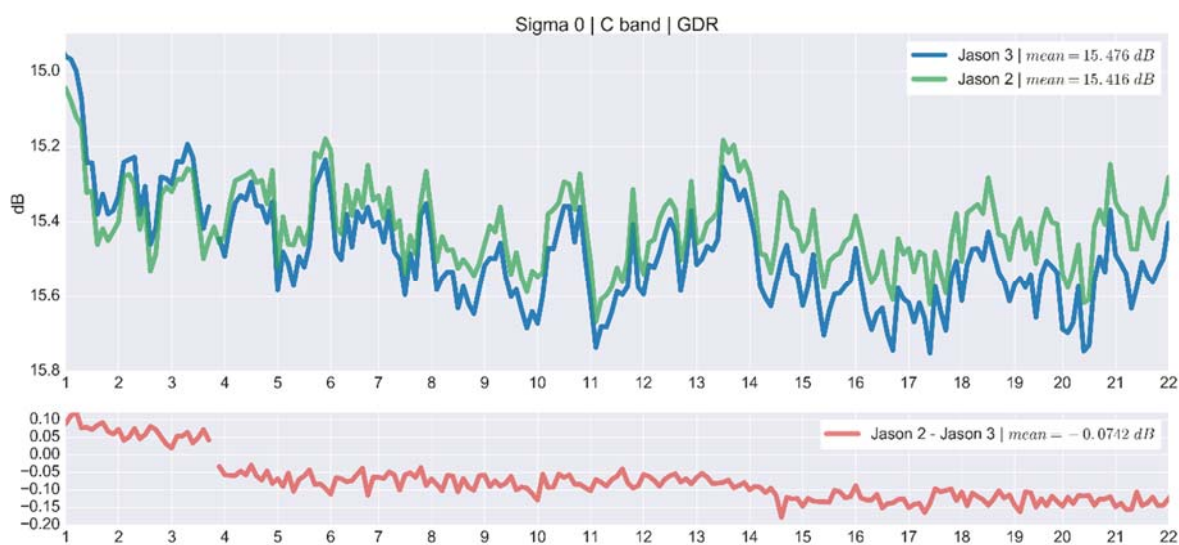


Figure 27: Daily monitoring of Sigma 0 for Jason 3 and Jason 2 in C band.

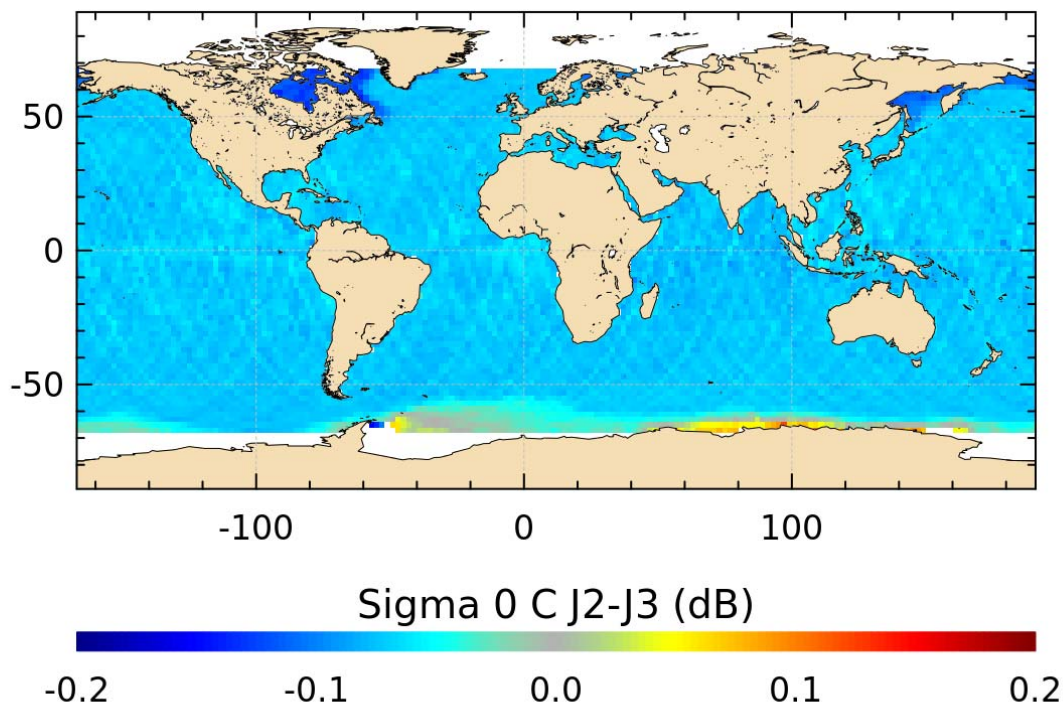


Figure 28: Mean of Jason 2-Jason 3 differences from cycle 0 to 22, C band.

#### 4.4. Significant Wave Heights

Significant wave heights present an excellent consistency between Jason 3 and Jason 2. (figure 29 and figure 31), and are very stable in time.

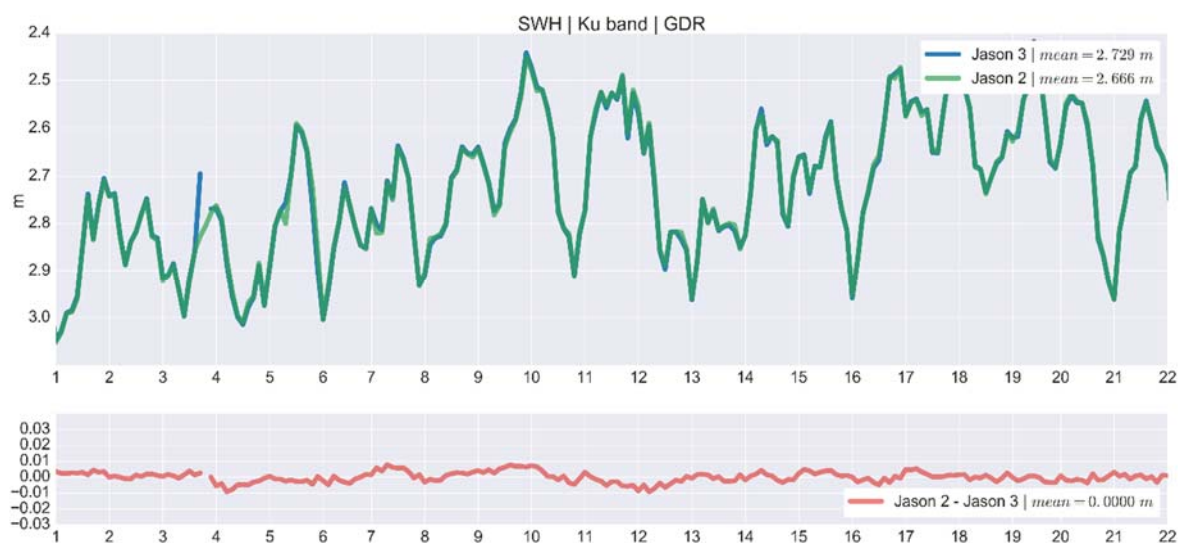
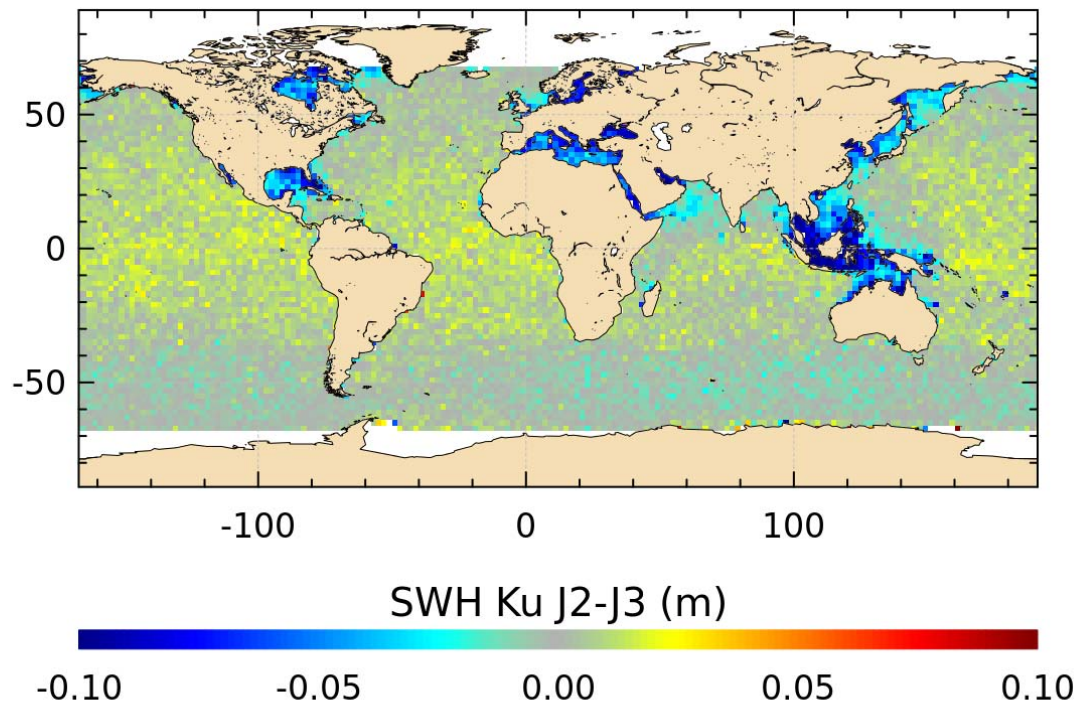


Figure 29: Daily monitoring of Significant Wave Heights for Jason 3 and Jason 2 in Ku band.



**Figure 30: Mean of Jason 2-Jason 3 differences from cycle 0 to 22, Ku band.**

The maps highlight some signals especially in Mediterranean Sea, in Gulf of Mexico and Indonesia where signatures are inverted whether Ku band or C bands is used. Such small geographical patterns could be related to the LUT applied on both missions, however these are areas with small SWH (< 1m) and where altimeter performance is not guaranteed.



**Figure 31: Daily monitoring of Significant Wave Heights for Jason 3 and Jason 2 in C band.**



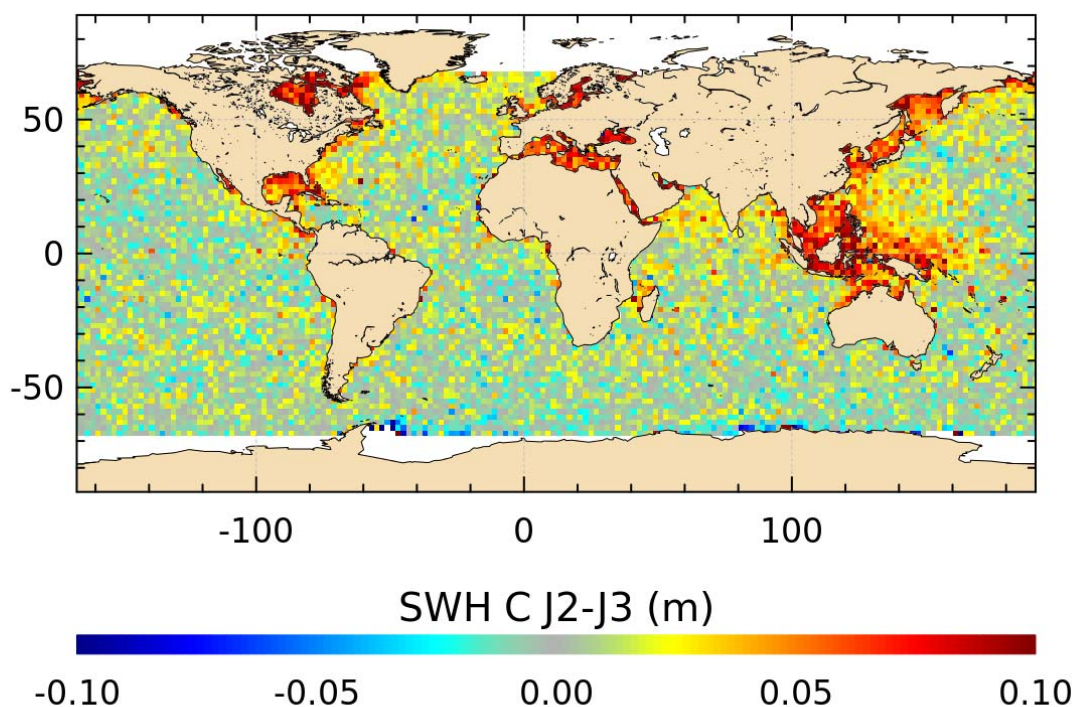


Figure 32: Mean of Jason 2-Jason 3 differences from cycle 0 to 22, C band.

#### 4.5. Dual frequency ionosphere correction

The dual frequency ionosphere corrections derived from the Jason-3 and Jason-2 altimeters shows a mean difference of about 0.55 cm (figure 33, top).

Until the LUT changes that occurred during cycle 14 (for O/IGDRs), the mean bias between the two missions was 1 cm (for O/IGDRs); it turns then to 0.55 cm following “jumps” of Ku range (5 mm), C Range (1.5 cm) and Sea state bias (0.1 mm). This event has an impact on Sea Level Anomalies retrieved from OGDRs and IGDRs products (Figure 33 bottom). For GDR products the same LUT were used for the whole mission period, therefore there is no jump (figure 33, top).





Figure 33: Daily monitoring of ionosphere correction for Jason 3 and Jason 2: in GDR mode (top) and in IGDR mode (bottom).

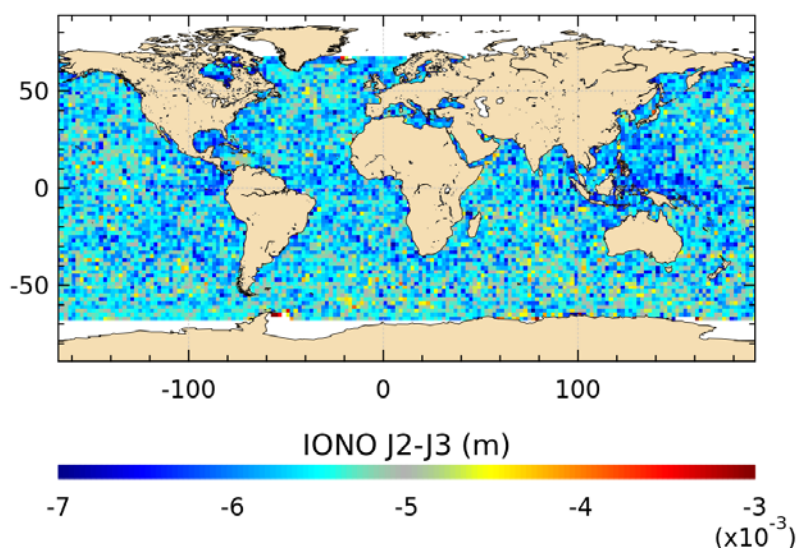


Figure 34: Mean of Jason 2-Jason 3 differences from cycle 0 to 22.



The map of differences between Jason2 and Jason 3 present small geographic variations about  $\pm 1.5$  mm.

#### 4.6. AMR Wet troposphere correction

In order to access to radiometer wet troposphere correction, liquid water content, water vapour content and atmospheric attenuation, Jason 3 uses a three-frequency AMR radiometer (18.7, 23.8 and 34.0 GHz), similar to the one used on board of the Jason 2 platform.

To compare Jason 3 and Jason 2 AMR the difference between wet tropospheric correction computed with AMR and wet tropospheric correction from ECMWF model is used.

Jason 3 AMR correction has a drift of more than half a millimetre per cycle for O/IGDRs, that is routinely monitored by JPL instrument expert team. Impact of drift is corrected through ground calibration (ARCS), also accounting for cold sky calibration. The first ARCS calibration is visible on figure 35, where a jump happens at the end of cycle 17.

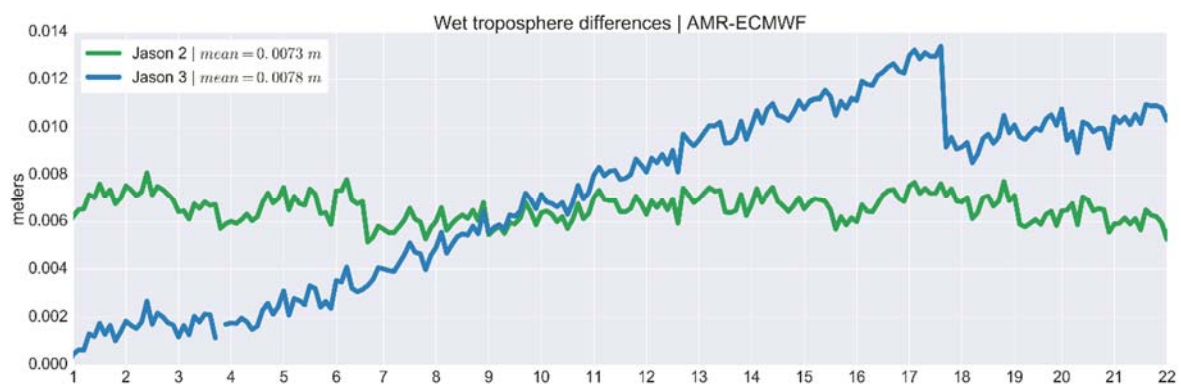


**Figure 35: Daily monitoring of wet tropospheric differences for Jason 3 and Jason 2, IGDR mode.**

In GDR mode, ARCS calibration is applied from cycle 0 which allows to correct the drift (figure 36); Jason 3 AMR-ECMWF model daily difference is 7.3 mm whereas it is 5.3 mm for Jason 2. Though the Jason 3 radiometer wet troposphere correction is more stabilized for GDRs, Jason 3 and Jason 2 do not have exactly the same behaviour, with an inflexion point around cycle 13.

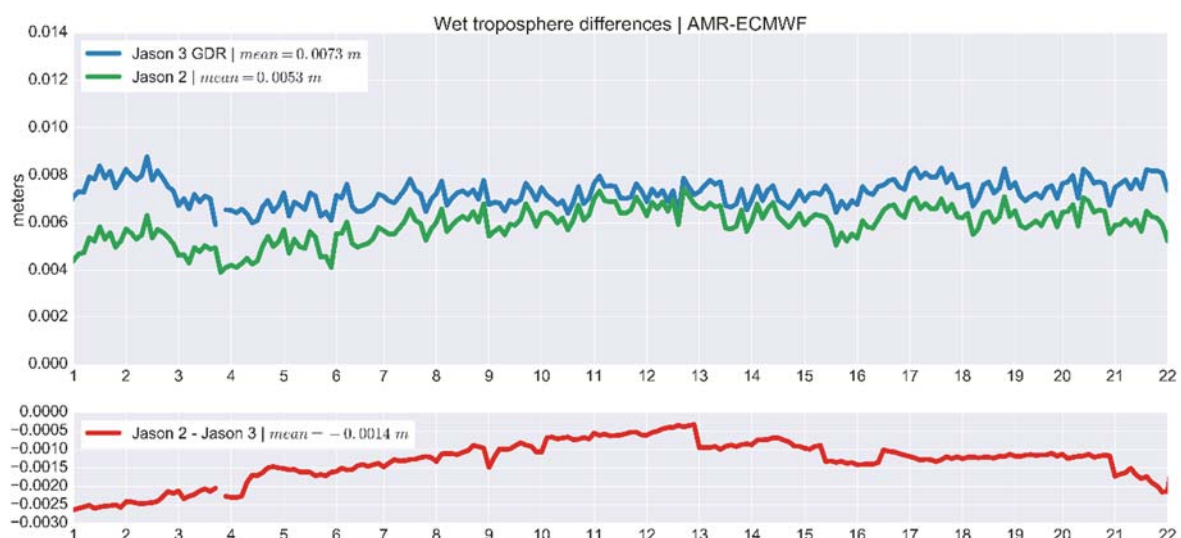


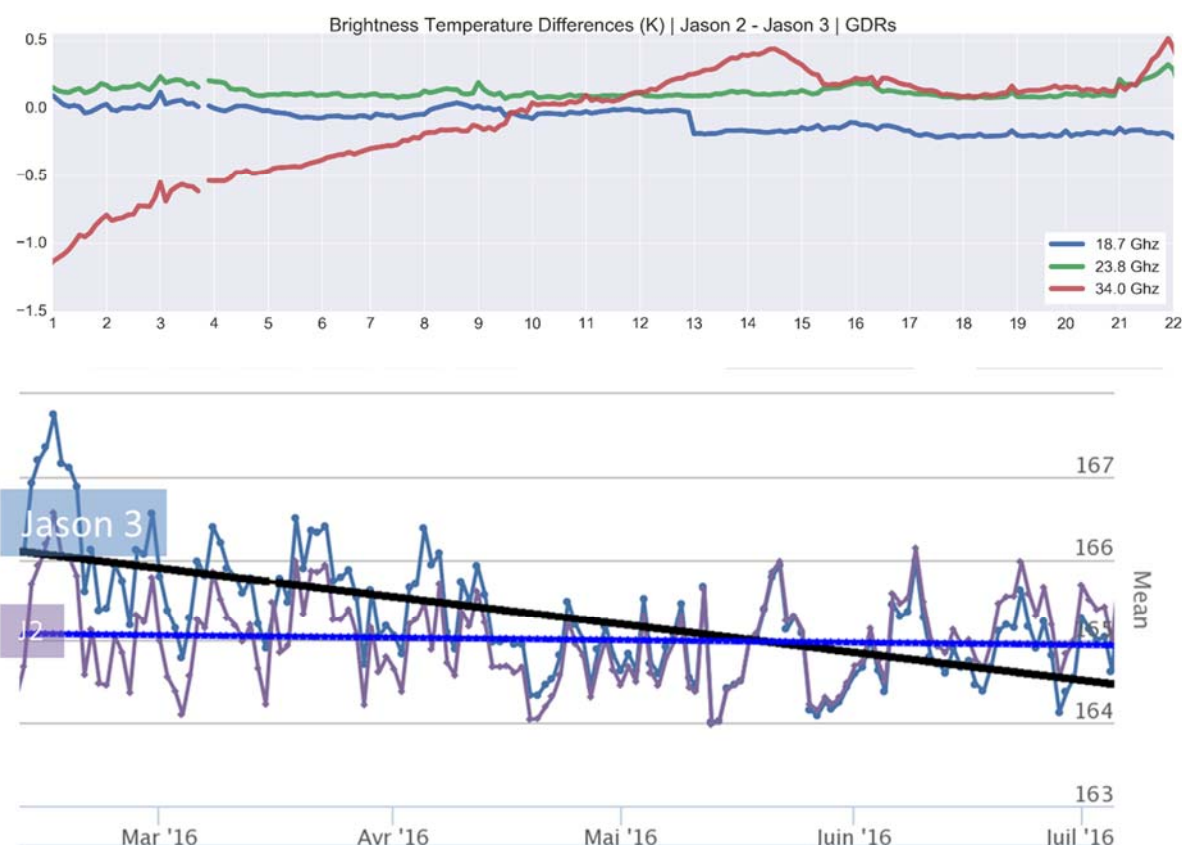
**Figure 36: Daily monitoring of wet tropospheric correction for Jason 3 and Jason 2, GDR mode.**



Actually the inflexion point is due to a Jason 2 radiometer 18.7Ghz channel calibration on cycle 293 (that is to say cycle 13 for Jason 3), which is also visible as a jump in the differences (Jason 2 - Jason 3) from figure 36 and figure 37.

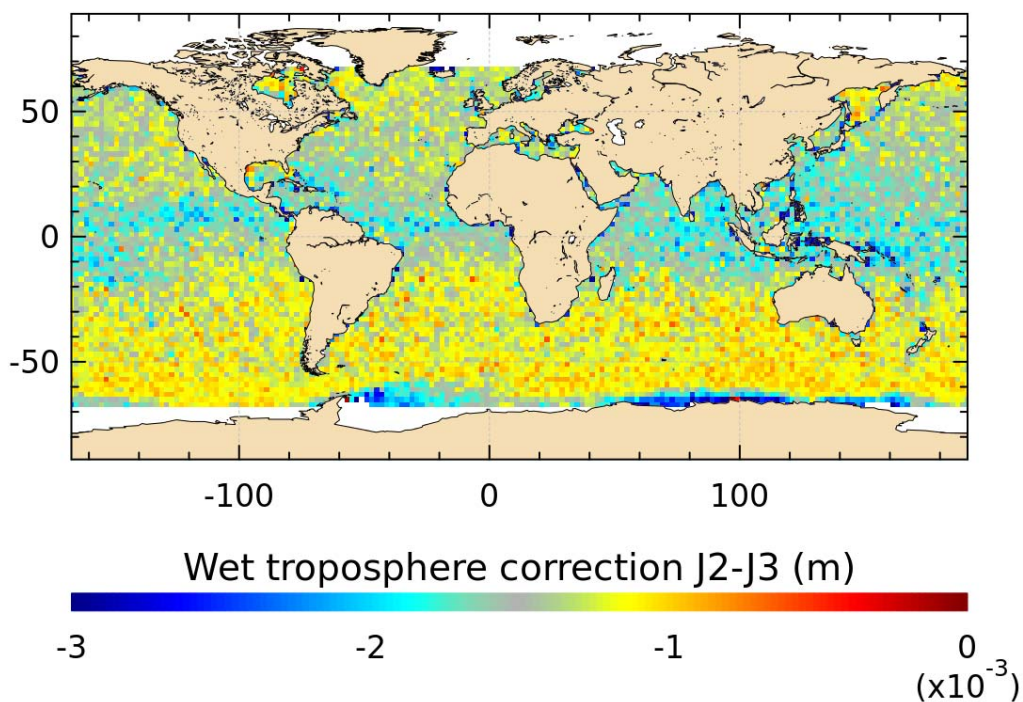
Focusing on brightness temperatures a residual drift can be observed on 34Ghz channel (figure 37, top) until cycle 14; this can be attributed to Jason 3 (figure 37, bottom, black linear regression plot) but its impact on wet tropospheric correction on GDRs is largely reduced and not comparable with IGDRs.

The map of differences (Jason 2 - Jason 3) highlights geographic patterns in agreement with wet tropospheric repartition, with very small residual signal ( $\pm 1$  mm, figure 38).



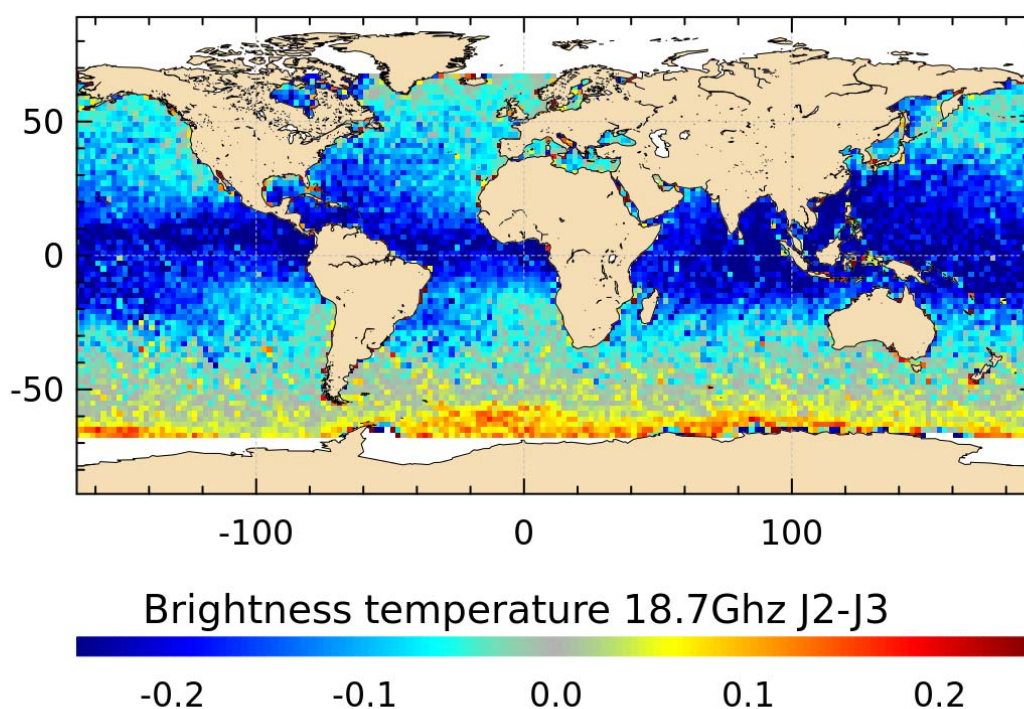
**Figure 37: Daily monitoring of brightness temperatures and differences between Jason 3 and Jason 2, GDR mode.**





**Figure 38: Mean of Jason 2-Jason 3 differences from cycle 0 to 22.**

The maps of brightness temperature differences highlight a good consistency between the Jason 3 and Jason 2 instruments with low differences of  $\pm 0.5\text{K}$ .



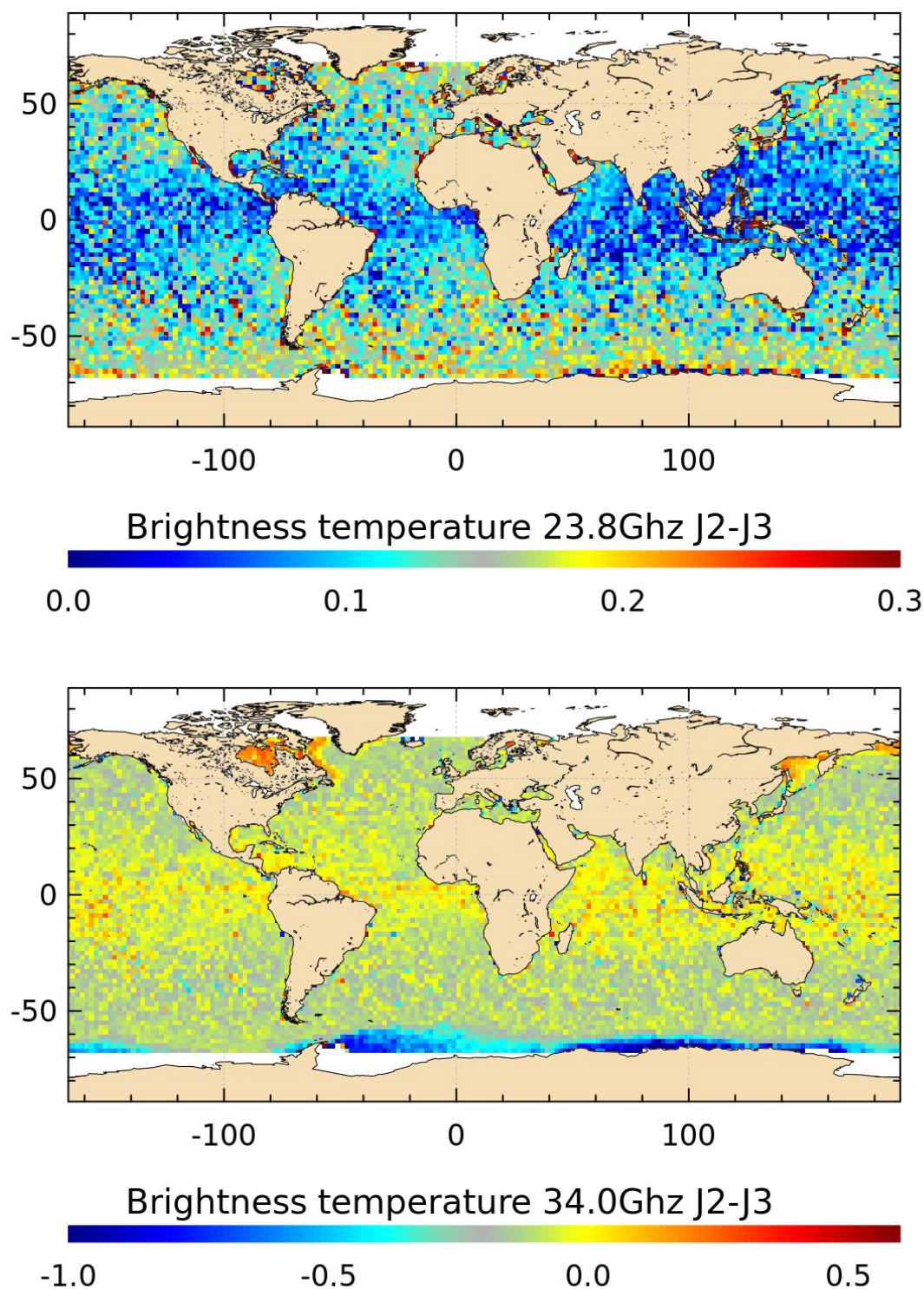


Figure 39: Mean of Jason 2-Jason 3 Tb differences (K) from cycle 0 to 22.

#### 4.7. Wind speed

Jason 3 and Jason 2 present very close results in terms of wind speed, and Jason 2 provides higher wind values than Jason 3 (7.66 vs 7.60 ms<sup>-1</sup>, figure 40).





The difference between the two missions is  $0.238 \text{ ms}^{-1}$  and can be separated in two phases: before and after GPS upload. The GPS upload occurred on March, 15<sup>th</sup> 2016 (Cycle 3) and corrected the square of nadir angle, that is to say the mispointing of the platform. Then from the restart of data production (March 18<sup>th</sup>) mispointing was set to value close to zero, which increases the  $\sigma_0$  and decreases the wind speed.

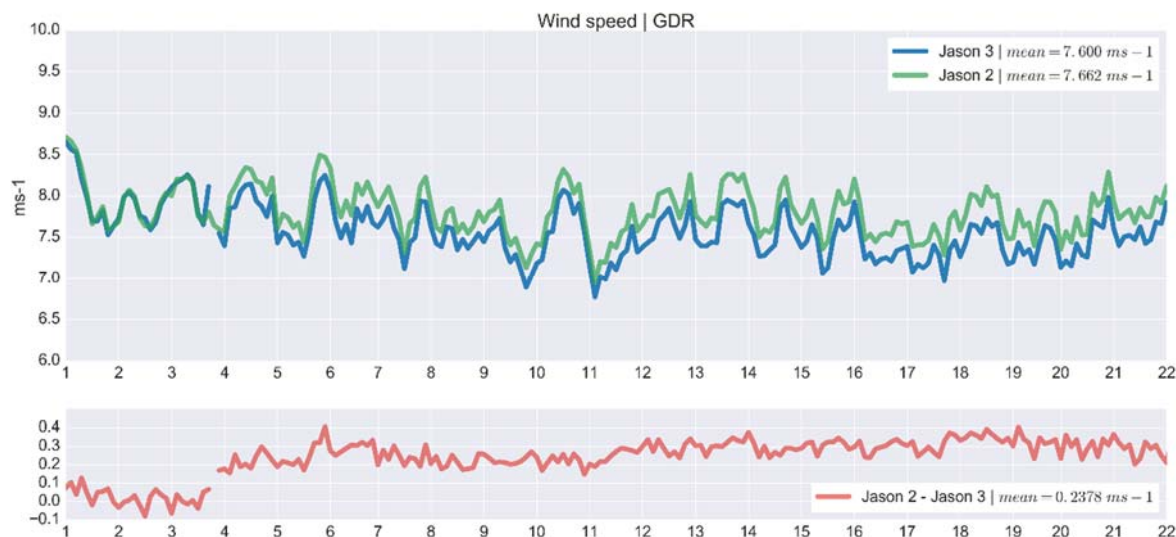


Figure 40: Daily monitoring of wind speed for Jason 3 and Jason 2.

The map (figure 41) highlights some geographic patterns where Jason 2 is higher than Jason3: these are areas of strong winds.

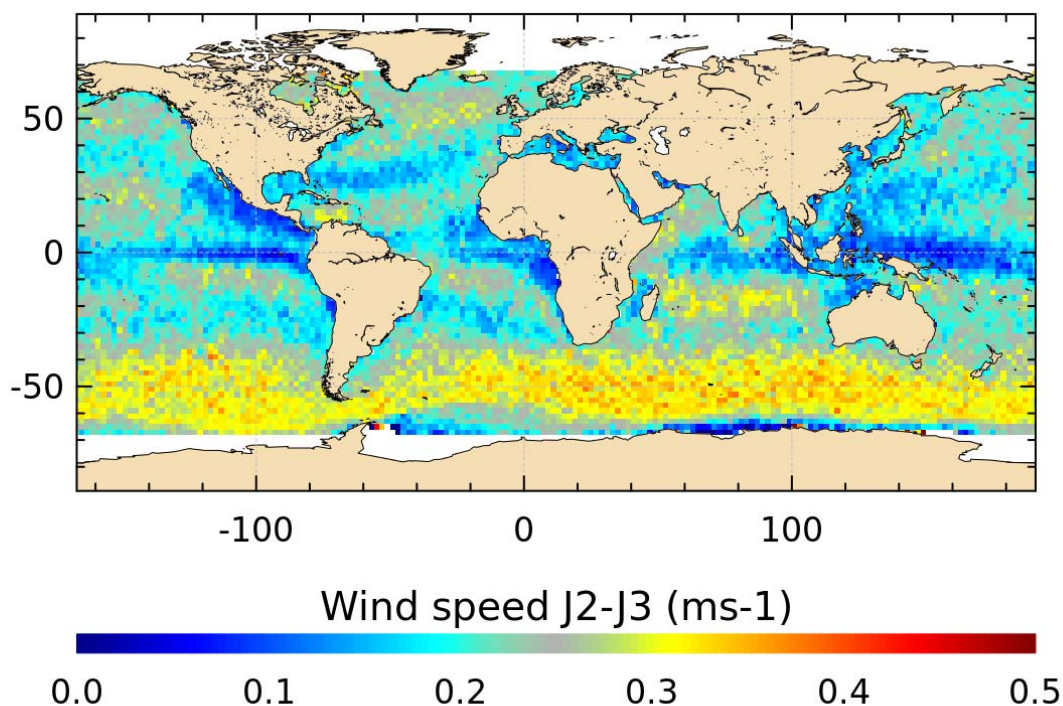


Figure 41: Mean of Jason 2-Jason 3 differences from cycle 0 to 22.



## 4.8. Sea state bias

Sea state bias (SSB) in Ku band from Jason 3 (8.5 cm) and Jason 2 (8.4 cm) present an excellent agreement both in average and in standard deviation (4.7 cm vs 4.6 cm, respectively).

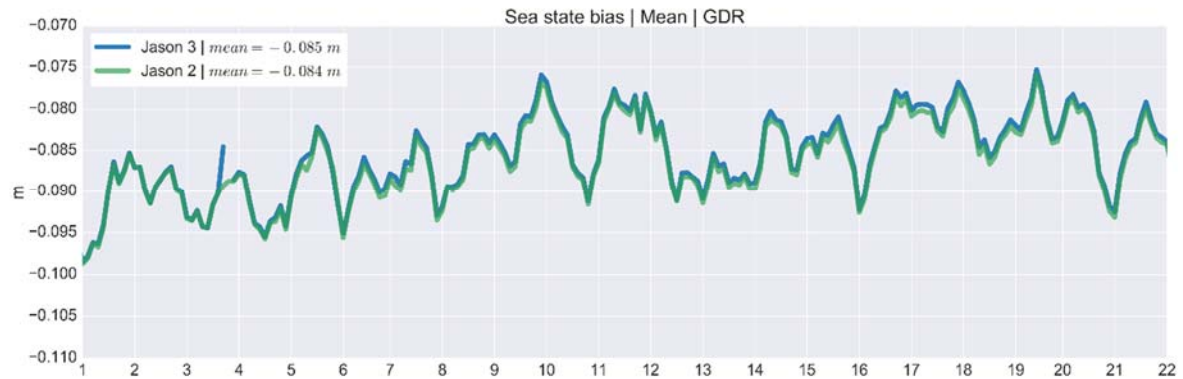


Figure 42: Daily monitoring of sea state bias for Jason 3 and Jason 2.

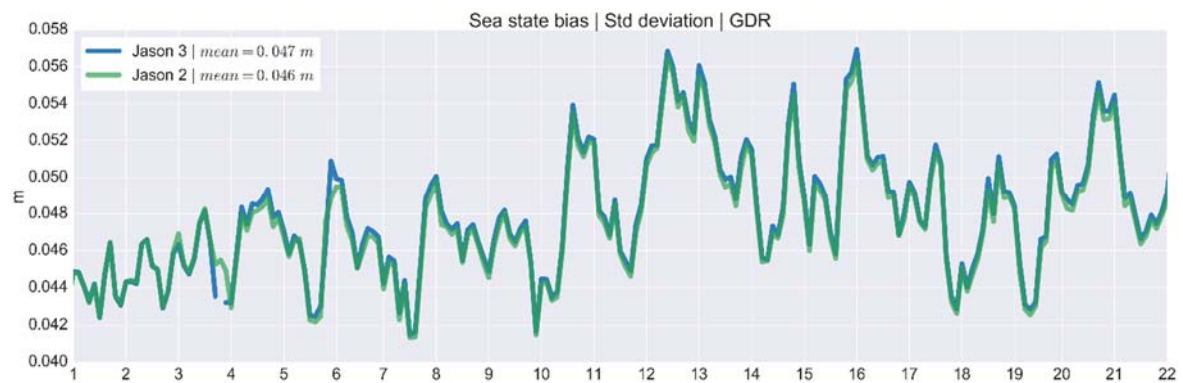


Figure 43: Daily monitoring of sea state bias standard deviation for Jason 3 and Jason 2.



## 5. Sea Surface Height crossover analysis

SSH crossover differences are the main tool to estimate the whole altimetry system performances, as they allow to analyse the SSH consistency between ascending and descending passes. In order to reduce the impact of oceanic variability, crossovers are selected with a maximum time lag of 10 days. This gives a measure of the performance on mesoscale time and spatial scales.

Mean and standard deviation of SSH crossover differences are computed from the valid data set, that is to say after selection and editing steps. In order to monitor the performances over stable surfaces, additional editing is applied to remove shallow waters (bathymetry above -1000m), areas of high ocean variability (variability above 20 cm rms) and high latitudes ( $> |50|$ deg). SSH performances are then always estimated with equivalent conditions.

The main SSH calculation for Jason 3 and Jason 2 are defined below.

$$\text{SSH} = \text{Orbit} - \text{Altimeter Range} - \Sigma \text{ Correction}$$

With

**Orbit**=CNES POE-E (standard E) for Jason 3 and Jason 2

**$\Sigma$  Correction** = Dry troposphere correction + Dynamical atmospheric correction + Radiometer wet troposphere correction + Ionosphere correction + Non parametric sea state bias correction + Ocean tide correction (including loading tide) + Earth tide height + Pole tide height

### 5.1. Mean of SSH crossover differences

The cycle by cycle mean of SSH differences (figure 43) respectively for Jason 3 and Jason 2 are in good agreement (-0.12 cm vs -0.13 cm) and do not highlight any anomaly.

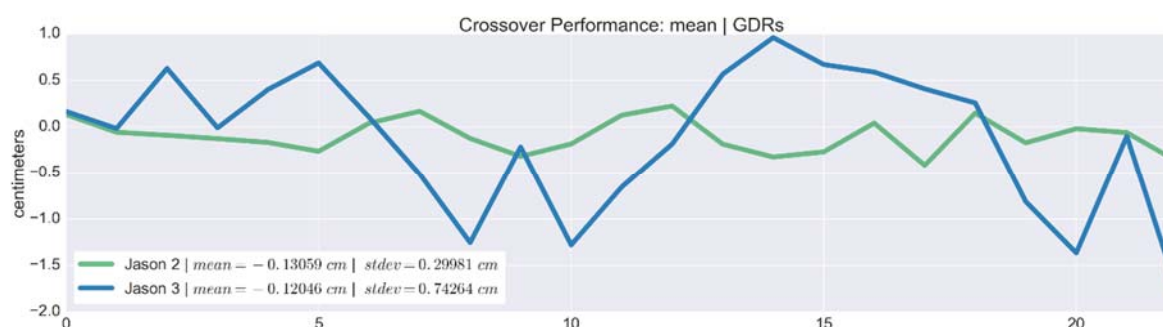


**Figure 44: Cyclic monitoring of crossover mean SSH differences for Jason 3 and Jason 2. Only data with  $\text{abs}(\text{latitude}) < 50$ , bathymetry  $< -1000\text{m}$  and low oceanic variability were selected.**

The map of mean SSH crossover differences (figure 45, top) highlights different geographic pattern between Jason 3 and Jason 2 in IGDR mode: for Jason 2 it is higher in southern Atlantic and northern Pacific, and lower in southern Pacific. These differences are significantly reduced for the two missions in GDR mode (figure 45, bottom). More generally both for Jason 3 and Jason 2 the performance at crossover is improved in GDR regarding to IGDR.

The mean of SSH differences for Jason 3 presents larger values (more than 1.5cm observed on cycle 22, under investigation).



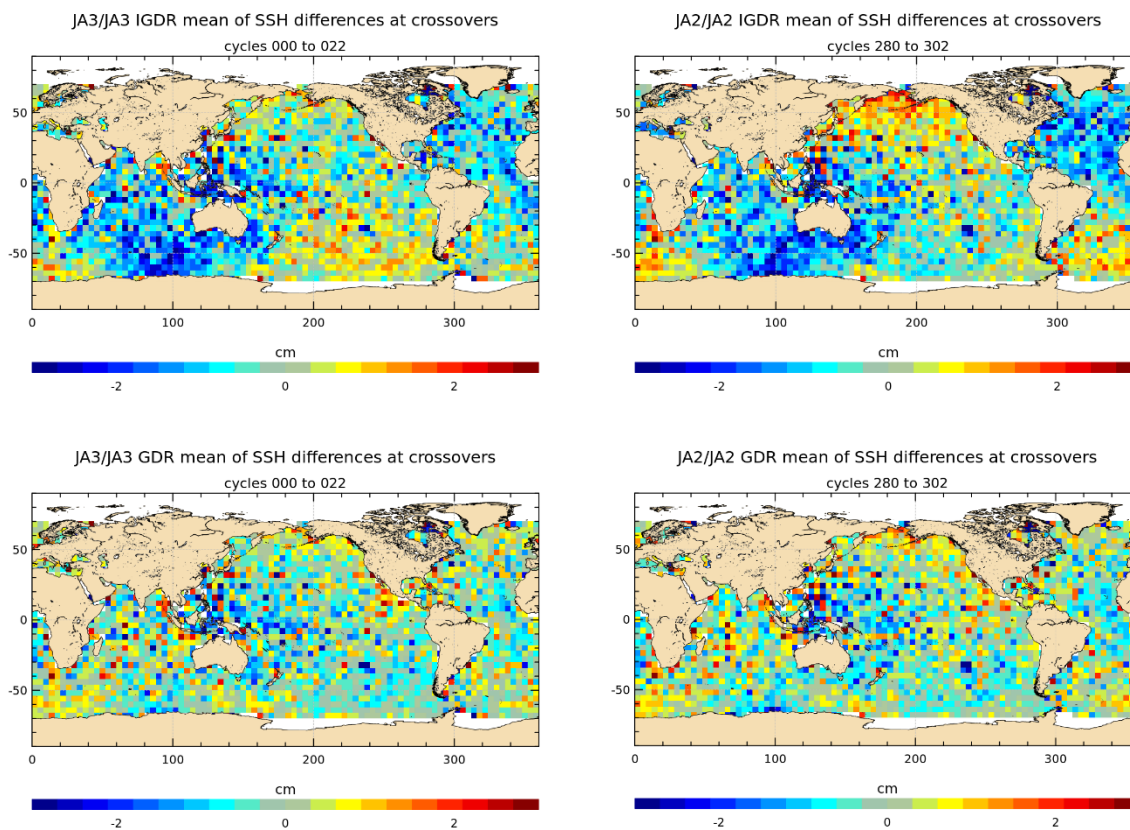


**Figure 45: Map of crossover SSH differences Jason 3 vs Jason 3 for cycle 22.**

The following figures (46 & 47) illustrate the performance of O/I/GDR at crossover focused on the first five cycles. The quality in crossover metrics is increasing going from OGDR to IGDRs, thanks to orbit improvements.

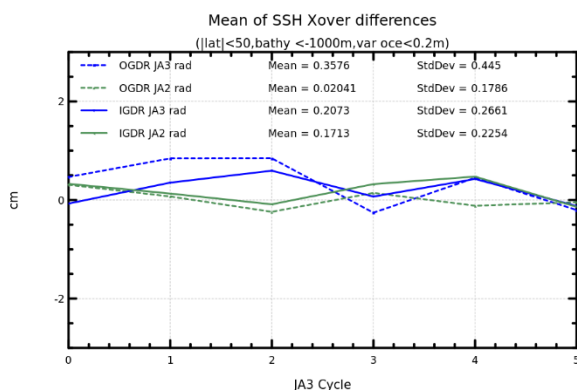


Figure 46: Comparison of mean SSH crossover differences between OGDR and IGDR for Jason 3 and Jason 2 during the first 5 cycles.

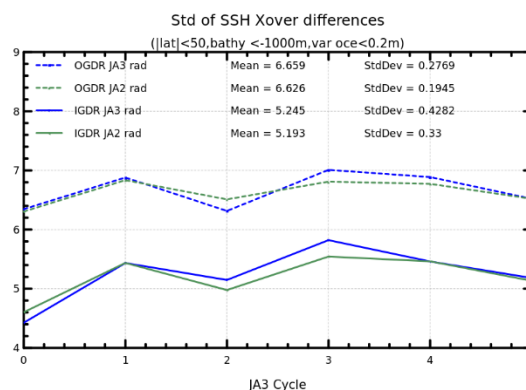


Figure 47: Comparison of SSH standard deviation crossover differences between OGDR and IGDR for Jason 3 and Jason 2 during the first 5 cycles.

## 5.2. Mean of SSH crossover differences between Jason 3 and Jason 2

Dual-mission crossover performances are computed between Jason 3 and Jason 2. Mean SSH differences at Jason 3/Jason 2 crossovers is 3cms in average, which is conform to the observed mean bias of 3cms between the two missions (figure 47). The geographical patterns indicate some hemispheric biases, positive to the west, negative to the east; they correspond to orbital signatures observed on sea surface heights (figure 51&52).

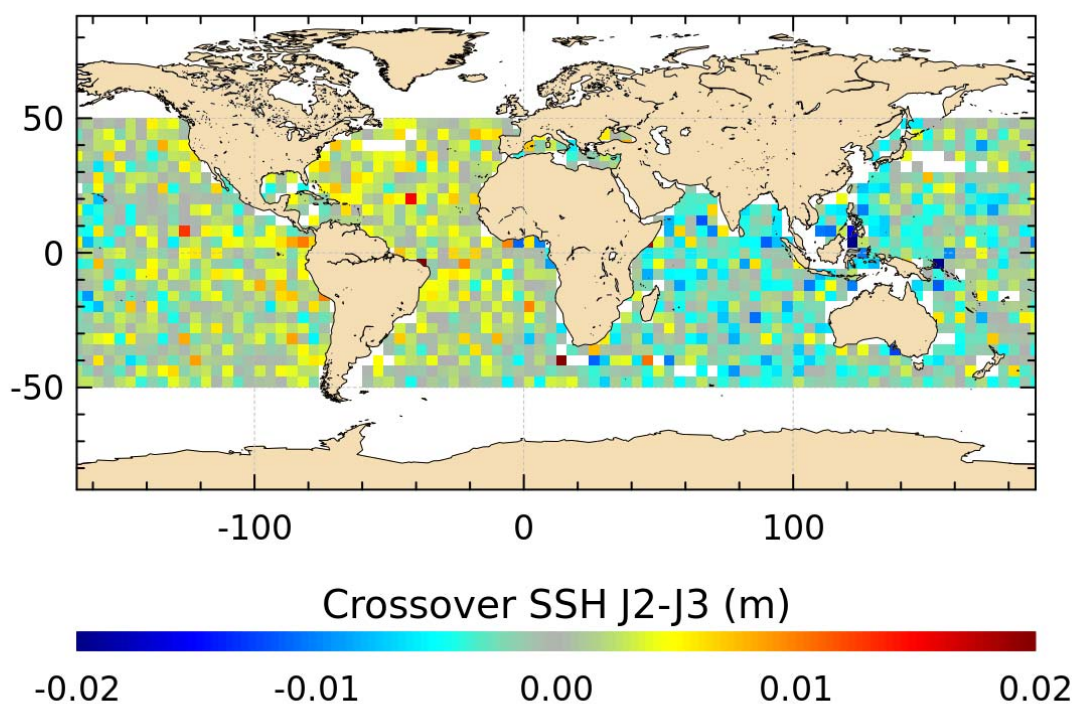


Figure 48: Map of crossover SSH differences Jason 3 vs Jason 2 from cycle 0 to cycle 22.



Considering the cycle by cycle mean of SSH differences (figure 48) between Jason 3 and Jason 2 at each crossover point, this is quite stable and around 2.97 cm in average.

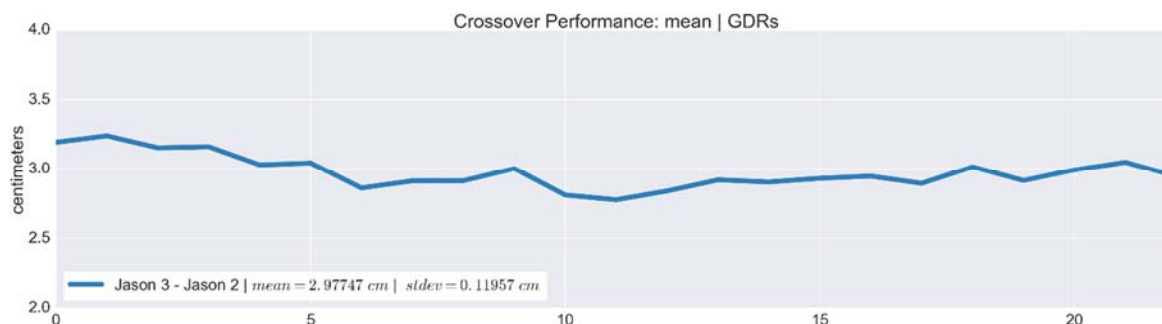


Figure 49: Cyclic monitoring of crossover mean SSH differences Jason 3 - Jason 2

### 5.3. Standard deviation of SSH crossover differences

The cycle by cycle standard deviation of SSH crossovers differences are plotted for Jason 3 and Jason 2 in figure 50 after applying geographical criteria selection (bathymetry, latitude, oceanic variability) as defined previously. Both missions show very good performances (5.03 cm for Jason 3, 4.93cm for Jason 2) and are stable in time. No anomaly is detected.

Note that during the formation flight of Jason 1 with TOPEX/Poseidon (2002) the same statistics using Jason-1 was close to 6.15 cm. Improvements are due to new retracking algorithms, new geophysical corrections (oceanic tidal, dynamic atmospheric correction, ...) and new orbit calculations.

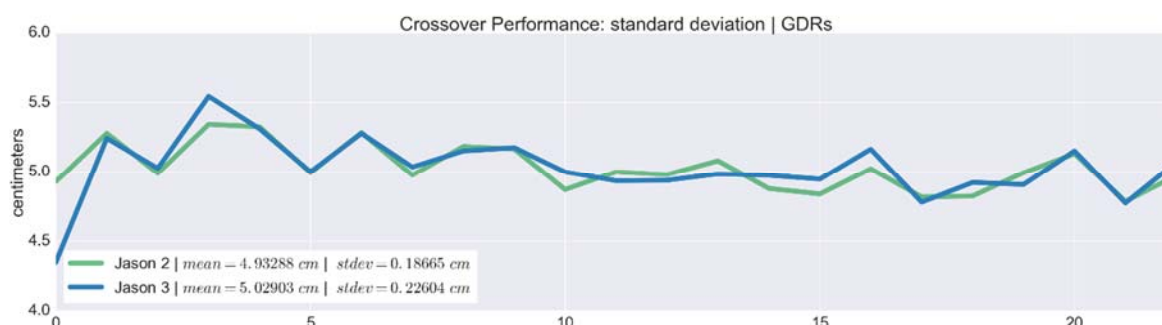


Figure 50: Cyclic monitoring of crossover standard deviation SSH differences for Jason 3 and Jason 2

## 6. Sea Level Anomalies (SLA) along-track analysis

The Sea Level Anomalies (SLA) are computed along track from the SSH minus the mean sea surface with the SSH calculated as defined in previous section 5.1 :

$$SLA = SSH - MSS(CNES-CLS2011)$$

SLA analysis is a complementary indicator to estimate the altimetry system performances. It allows us to study the evolution of SLA mean (jumps detection, abnormal trend or geographically correlated biases) and also the SLA variance for long term stability. During formation flight, SLA from the two missions are compared.

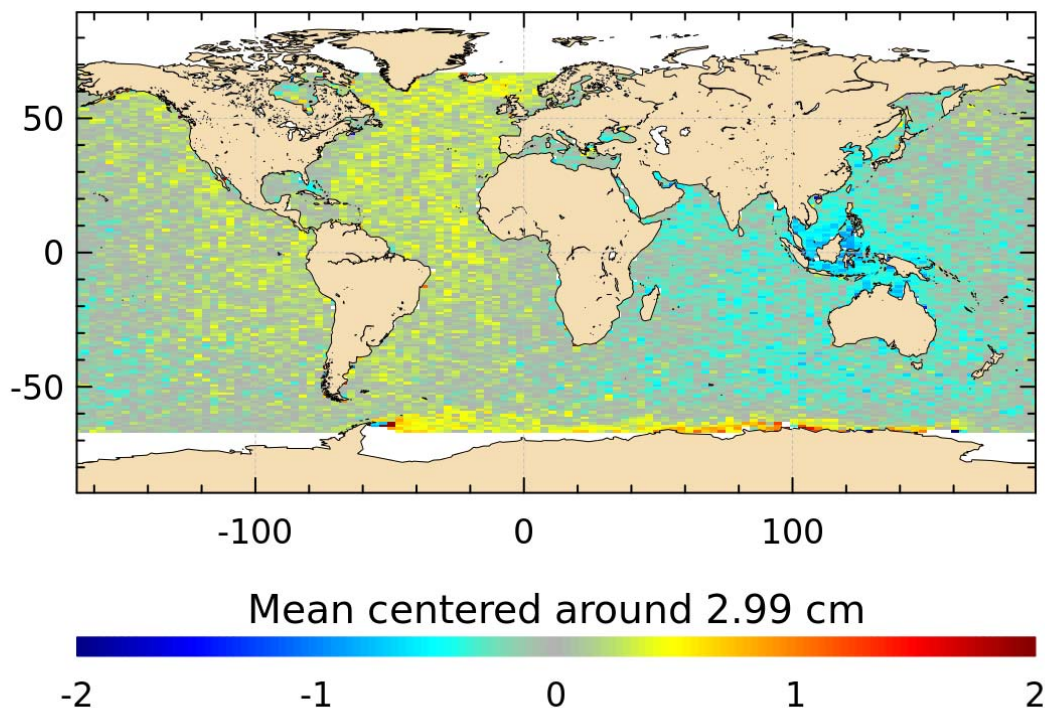


Figure 51: Mean of Jason 2-Jason 3 SLA differences cumulated over cycle 0 to 22.

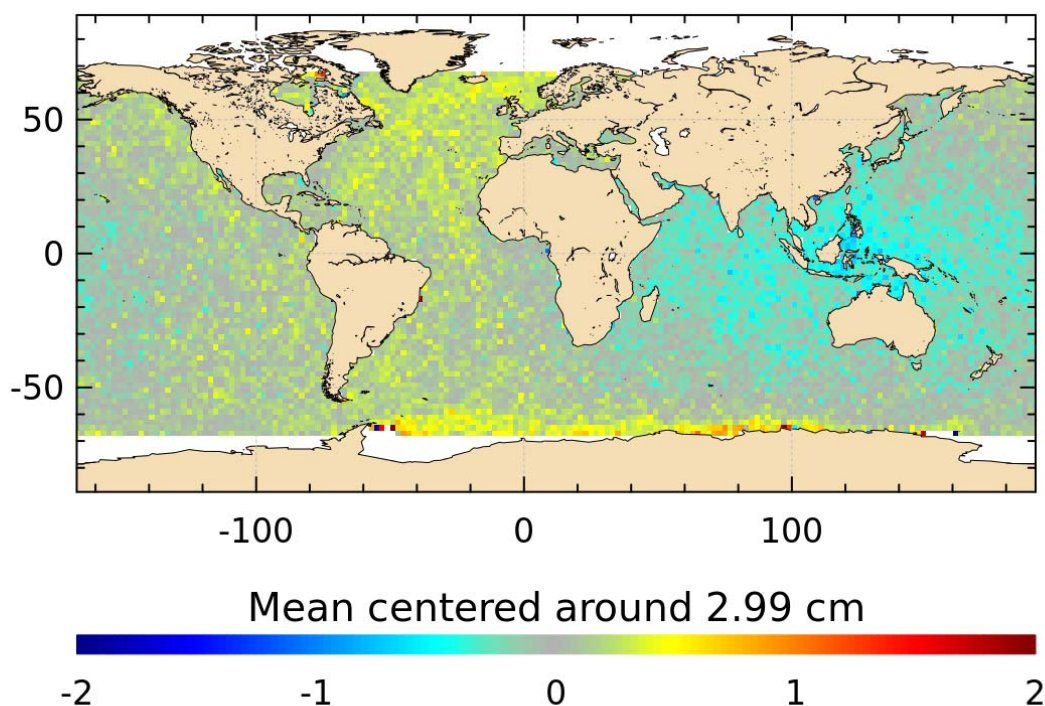


Figure 52: Mean of Jason 2-Jason 3 non corrected SLA (orbit - range - MSS) differences cumulated over cycle 0 to 22.





Figure 51 and 52 maps depict a geographic signature with a weak east/west bias lower than 1 cm. In addition, positive differences are stronger in eastern Pacific & Atlantic and negative differences are stronger in western Pacific & Indian.

One part of the geographic biases can be attributed to the range, as Jason 2 and Jason 3 have a different behaviour observing lower sea states, the other part of differences is due to orbit.

Orbit estimates is perturbed by South Atlantic Anomaly (SAA); the yellow/blue patches are remaining signals of the perturbations induced by SAA, but their magnitude of order ( $\pm 0.5\text{cm}$ ) is very small.

The monitoring of SLA difference highlights a very good agreement between Jason 2 and Jason 3. The mean bias between missions, estimated here using repeat-track analysis is 2.99 cm and is very stable (figure 52), whereas it is 3.39 cm in terms of standard deviation (figure 53).

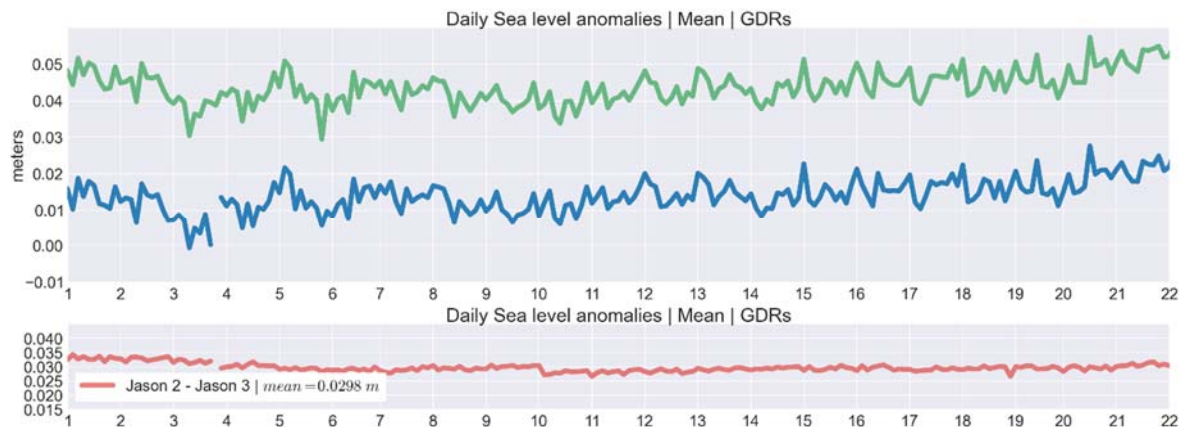


Figure 53: Daily monitoring of mean SLA and differences between Jason 3 and Jason 2.

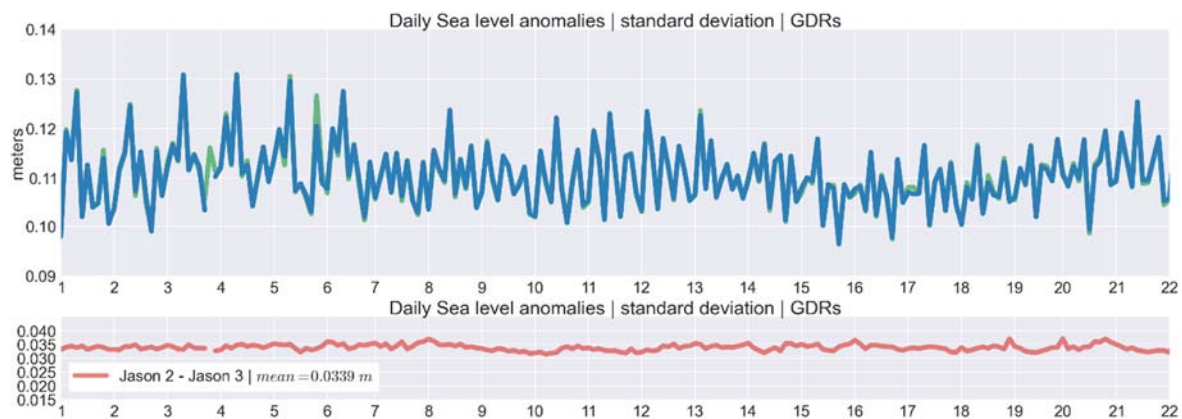
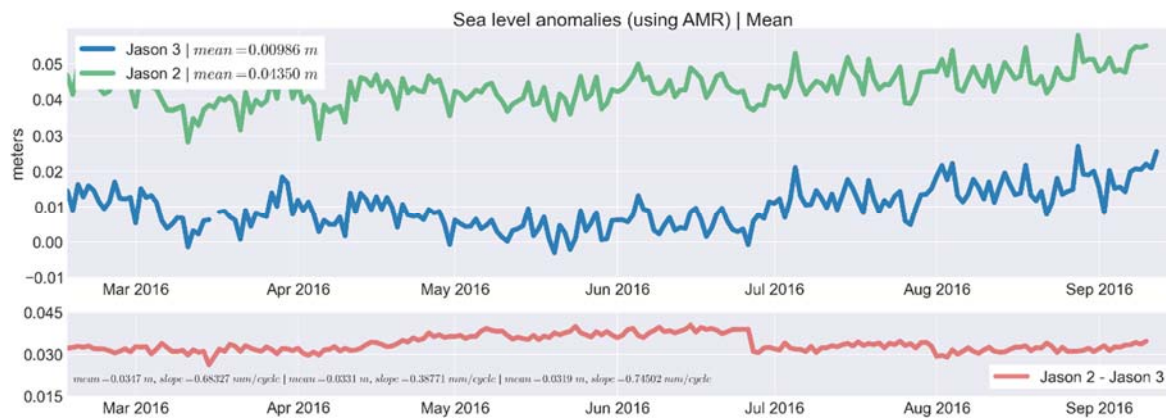


Figure 54: Daily monitoring of mean SLA and differences between Jason 3 and Jason 2.

In IGDR mode, some jumps are present on the SLA differences between Jason 2 and Jason 3: end of June 2016 (1 cm), due to CAL2 and LUT corrections changes, and end of July due to radiometer ARCS calibration (figure 55). They are neutralised when turning to GDR mode.



**Figure 55: Daily monitoring of mean SLA and differences between Jason 3 and Jason 2, IGDR mode.**



## 7. Mean Sea Level (MSL) calculation

Since 2016, Jason 3 become the reference altimetry mission to estimate the Global Mean Sea Level (GMSL), instead of Jason 2. Then Jason 2 and Jason 3 have to be interconnected, that is to say regional and global biases between missions have to be precisely estimated.

The method used to calculate the GMSL bias between two missions is only applicable to the mission on the TOPEX historical orbit: T/P, Jason-1, Jason-2, Jason-3; this takes advantage of the verification phase between both missions.

A common period of 11 cycles is selected within the verification phase, centred on the middle of the period. Basically, the relative GMSL bias is then computed as the difference of both MSL series averaged over this common period. The final GMSL bias for each mission is the sum of the absolute GMSL bias of the previous mission with the relative of the following with previous one:

$$\text{bias GMSL (J3)} = \text{bias GMSL (J2)} + \text{relative bias (J3/J2)}$$

The sign of the GMSL bias checks this convention:

$$\text{Unbiased GMSL (J3)} = \text{GMSL (J3)} - \text{bias (GMSL J3)}$$

In the case of Jason 3, the period was centered on cycle 11 and going from cycle 6 to cycle 16. Then the estimated global bias is -2.5783 cm, where average is weighted by latitude - that is to say that the bias here is different from the previous bias estimates between Jason 2 and Jason 3.

The regional biases were estimated by using the first twenty SLA (JA2 - JA3) maps.

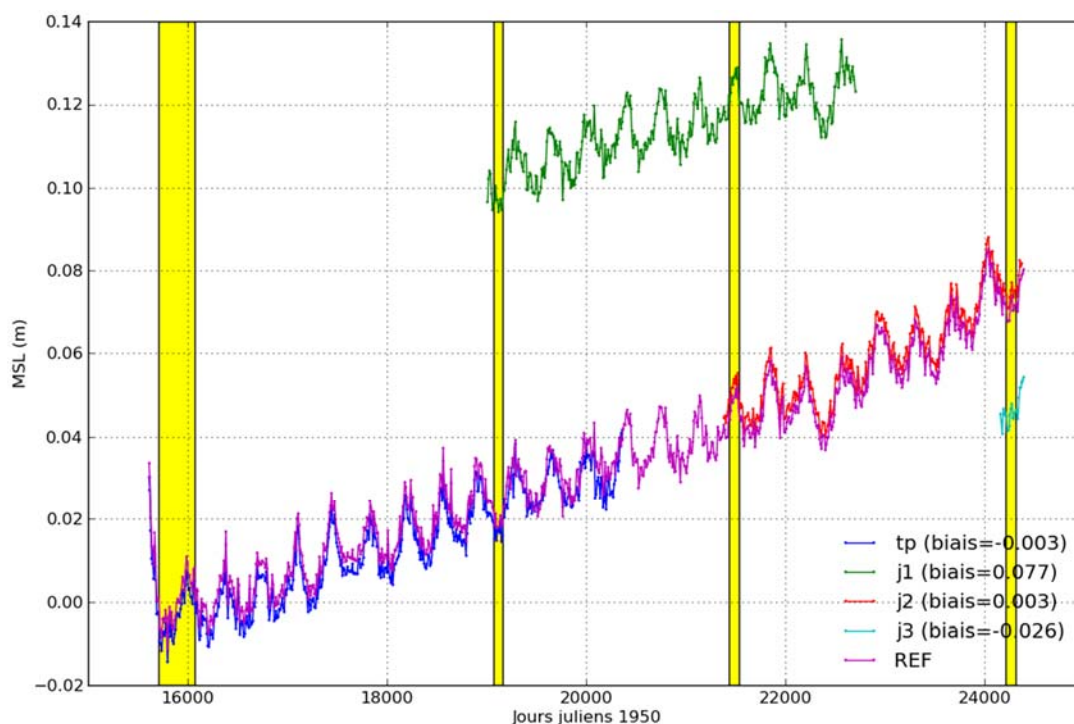


Figure 56: T/P, JA1,JA2,JA3 concatenated after bias correction

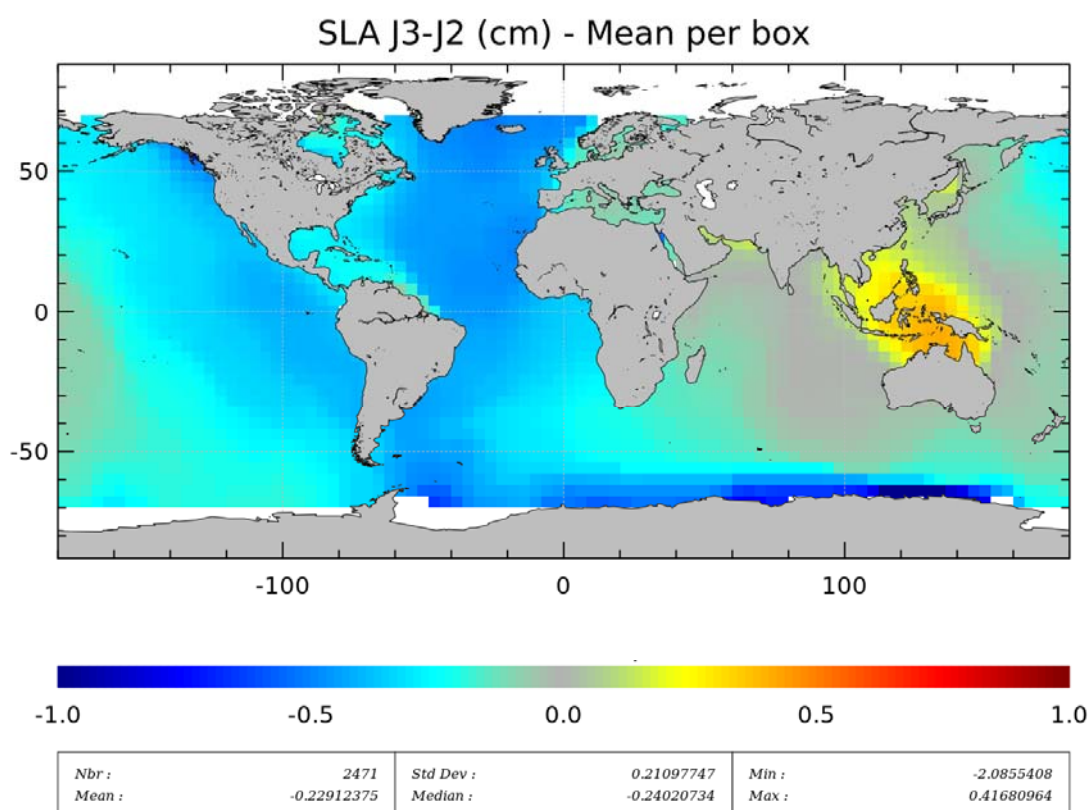


Figure 57: Regional biases between Jason 3 and Jason 2

## 8. Investigations

### 8.1. Altimetry errors for submesoscale

#### 8.1.1. Error description

The sea level content provided by most of the conventional altimeters in low resolution mode (LRM) does not allow the observation of ocean scales smaller than 80-100 km (Dibarboure et al., 2014 [1]). This limitation is mainly due to surface heterogeneities in the altimeter footprint (e.g. rain, sigma blooms) and the white noise level due to the instrumental noise and the measurement estimation. Hereafter, a quantification of these errors is presented.

A usual way to represent the error budget of altimeter missions at these small scales is to perform spectral analyses of sea-level anomalies. Such spectra based on Fourier's transform are plotted in Figure 58 for Jason-2, Jason-3 and SARAL/Altika at global scale and from high rate measurements. The noise level of each altimeter is easily deduced from the high frequency plateau of both missions. The white noise level is respectively estimated to 7.3 cm for Jason-2/Jason-3 and 5.4 cm for Altika, for significant wave height close to 2.7 m on average. This difference between both missions is mainly explained by the Altika high rate higher for Altika (40 Hz) than for Jason-2/Jason-3 (20 Hz). The noise level prevents the observation of small oceanic structures for distance on average close to 50 km for SARAL/Altika and 60 km for Jason-2/Jason-3. This distance is defined by the ratio between the oceanic signal slope and high frequency plateau equal to 1. This corresponds in Figure 58 to the X-axis of the intersection between the high frequency plateau and the oceanic slope (Dufaut et al., 2016 [2]).





Furthermore, a large energy bump for wavelengths higher than few kilometers and lower than 100 km is observed as well as for Jason-2/Jason-3 as for SARAL/Altika (Figure 58). Dibarboure et al., 2014 [1] described in details this signal and its origin. Basically, it is due to surface heterogeneities in the LRM footprint impacting altimetry measurements as for instance in areas impacted by rain cells or sigma bloom. The comparison of the observed SLA spectrum with the expected spectrum derived from the oceanic slope and the noise level (green, red and blue dash spectra in Figure 58) allows the quantification of this error. At 80 km, about 50% of additional energy is measured. Therefore, the addition of this error and the white noise prevents the observation of small oceanic scales lower than 80-100 km (on average) for all the LRM missions.

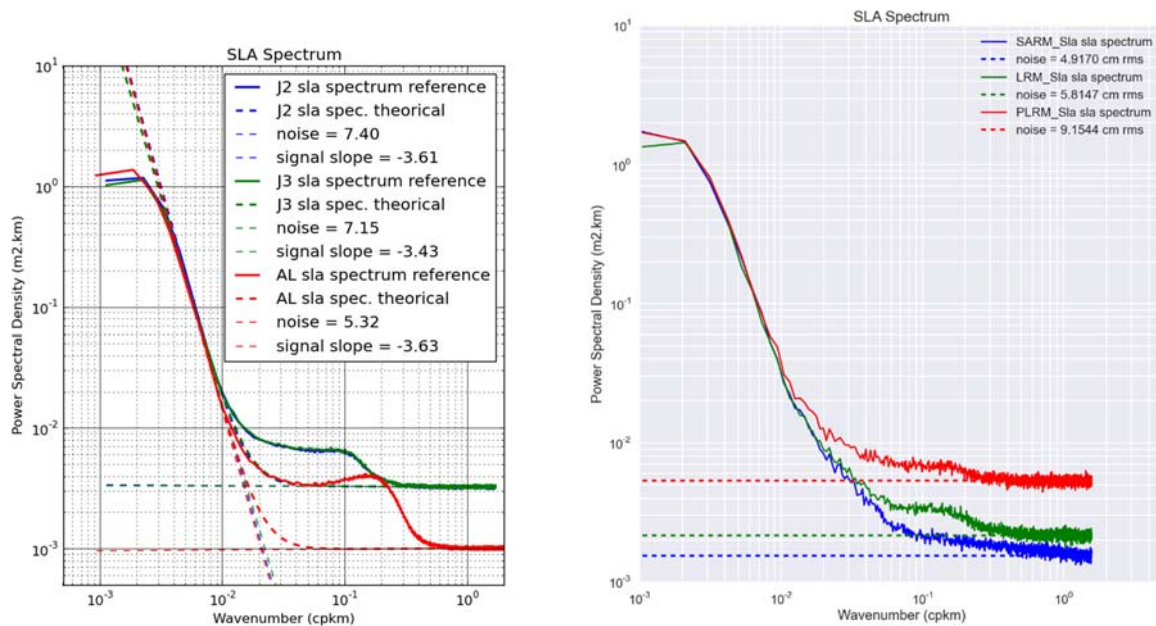


**Figure 58 : SLA spectra for Jason-2/Jason-3 and SARAL Altika from respectively 20 Hz and 40 Hz measurements (left) and from Sentinel 3A (right)**

### 8.1.2. Expected Improvements

The altimeter processing can have a strong impact on sea level performances at these small scales, as for instance the choice of retracking algorithms, empirical methods to reduce the altimeter noise or to remove spurious sea-level measurements. Furthermore, the improvements and benefits brought by Delay Doppler altimetry (or SARM) in terms of noise reduction and better across-track resolution allows avoiding this kind of artefact. In this way, the global SAR-mode coverage ensured by the recent Sentinel-3a mission (launched in February 2016), should significantly improve the observation and the understanding of small oceanic scales (figure 58).

Hereafter, two methods have been further investigated to improve LRM measurements at small oceanic scales:

1. The development of a better editing procedure adapted to the high rate measurements (20 Hz or 40 Hz). The schema below gives the principle of the method.
2. The application of the empirical noise reduction method developed by (Zaron et al [3]), based on the correlation between the altimeter range and significant wave height noise:  $\Delta SLA / \Delta SWH = a + b SWH$ .

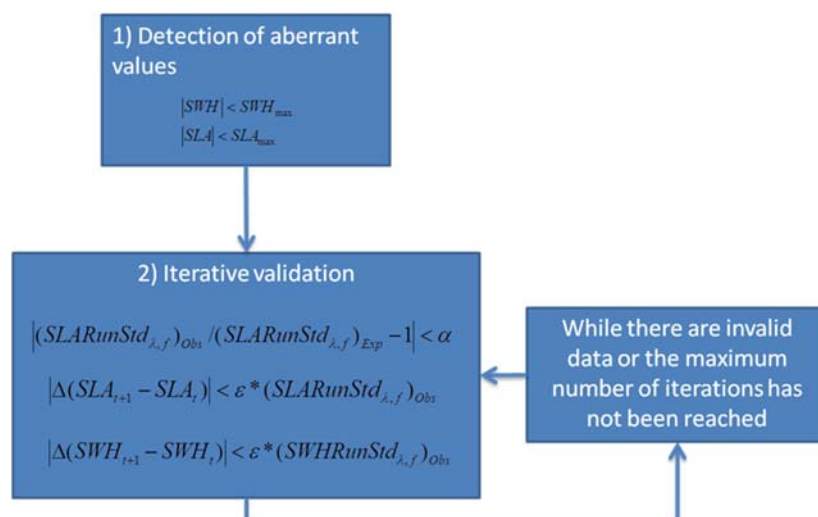


**Figure 59 : Editing procedure adapted to high rate measurements for Jason-2/Jason-3 and SARAL/Altika missions**

The impact of both new editing algorithm and Zaron's method (noted V1 hereafter) has been compared to Jason-2 data processed with a basic editing procedure (based on duplication of 1-Hz editing flag) and without any reduction flag (noted V0 hereafter).

Firstly, maps of variance reduction of SLA have been calculated filtering out along-track data lower than 200 km (Figure 60). Significant SLA variance reduction is observed especially in areas where waveforms are disturbed by rain cells and sigma bloom events. On average, at global scale, the variance is reduced by about 2 cm<sup>2</sup>. This statistic can reach 4-5 cm<sup>2</sup> in rain areas. The improvement in rain cells may be due to the new editing algorithm allowing a better detection of bad measurements. It is worth noting that about 3-4% of additional measurement have been removed (mainly in rain areas) compared to a classical 1-hz editing procedure.

Secondly, SLA spectra have been calculated for each V0 and V1 datasets (Figure 61). A significant white noise reduction is observed by about 40% thanks to the Zaron's method. This allows the reduction of the Signal Noise Ratio (SNR) distance from about 60 to 50 km. A reduction of the spectral "bump" - characterizing the LRM errors at small oceanic scales - is also observed for distances lower than 30 km (Figure 61 on right panel). However, the spectral bump is just slightly modified for distances between 30 and 80 km. Unfortunately, these distances are of main interest for submesoscale studies. This means that the improvements described here do not really improve the observations of mesoscale structures on average at global scale. However, in specific areas with small altimeter range noise (i.e. small SWH), observations of smaller oceanic structures are likely possible. It is also worth noting that SLA spectrum analyses with classical Fourier's transform only reflect the altimeter sea-level performances in areas with segment long enough (1000 km). In other words, this also means that SLA spectrum analyses are not adapted to measure the improvement in rain areas where segment are too short.

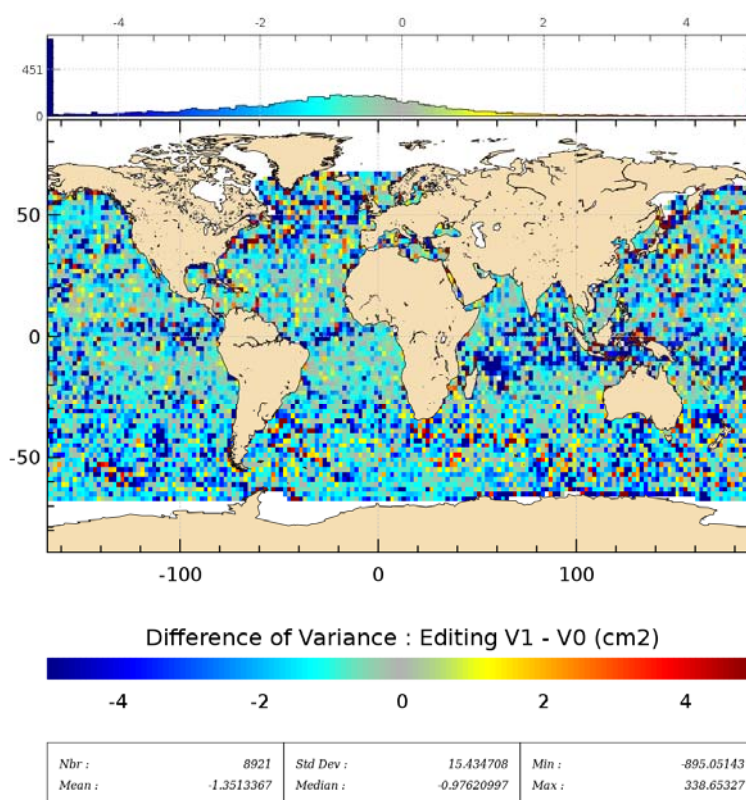


Figure 60 :: Map of SLA variance reduction applying new editing and Zaron's method (V1) compared to data processed with classical 1-Hz editing procedure (V0), after filtering out along-track data lower than 200 km.

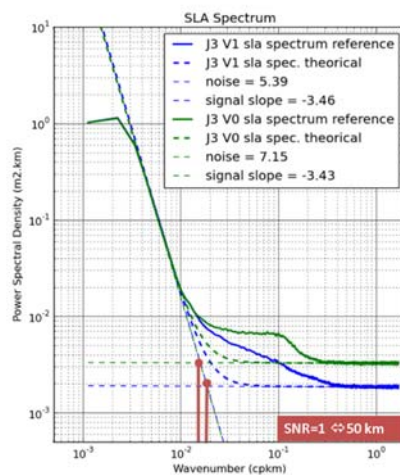


Figure 61: SLA spectra applying new editing and Zaron's method (V1) compared to data processed with classical 1-Hz editing procedure (V0) : classical power spectral density spectra with theoretical spectra superimposed (dashed lines) on left and spectra differences between classical and theoretical spectra on right. Theoretical spectrum is defined from the oceanic slope (as observed by model) and the white noise level (plateau).



## 9. Conclusion

Jason 3 was launched on January, 17th 2016. Since February 12th, Jason 3 was on its operational orbit following Jason 2 with 80 seconds delay on the same ground track. OGDR/IGDR products were opened to users end of June 2016, whereas the GDR products ("GDR-d") were available from November 2016 onwards (*NB: "GDR-T" are also equivalent to "GDR d"*).

The verification phase allowed extensive analysis and validation of the data, as both satellites observed the same geophysical phenomena until October 2<sup>nd</sup> when Jason 2 was moved to its interleaved ground track.

The flight formation phase has shown that Jason 3 data quality is excellent, at least of the same order as the Jason 2 one; data availability is excellent and similar between missions, as for the selection of valid data.

The altimetry parameter analysis highlights a similar behaviour compared to Jason 2. Some biases exist as between dual-frequency ionosphere correction (0.55cm), but they are stable.

A drift was observed on the radiometer in IGDR (between 0.5-0.6 mm per cycle), but was corrected for GDR product generation.

A jump on SLA (1 cm) was observed in IGDR after some changes on LUT corrections; this jump is no longer in GDR products, because the same new LUT corrections were applied from the beginning of GDR production.

The SSH performances analysed at crossovers between Jason-3 and Jason-2 presents excellent results. The consistency between both SLA is good with a small geographically correlated signal - lower than 0.5 cm in GDR - due to orbit estimation. SLA bias between Jason 2 and Jason 3 is 3cms. Jason 3 is now the reference mission to ensure the continuity of Global Mean Sea Level monitoring.





## 10. References

- [1] Ablain, M., A. Cazenave, G. Valladeau, and S. Guinehut. 2009 : A new assessment of the error budget of global mean sea level rate estimated by satellite altimetry over 1993-2008. *Ocean Sci*, 5, 193-201. Available at <http://www.ocean-sci.net/5/193/2009/os-5-193-2009.pdf>
- [2] Ablain, M., S. Philipps, 2006, Topex/Poseidon 2005 annual validation report, Topex/Poseidon validation activities, 13 years of T/P data (GDR-Ms).
- [3] Ablain, M., S. Philipps, M. Urvoy, N. Tran, and N. Picot (2012) Detection of Long-Term Instabilities on Altimeter Backscattering Coefficient Thanks to Wind Speed Data Comparisons from Altimeters and Models, *Marine Geodesy*, 35:51, 258-275. Available at <http://www.tandfonline.com/doi/pdf/10.1080/01490419.2012.718675>
- [4] Ablain, M., G. Larnicol, Y. Faugère, A. Cazenave, B. Meyssignac, N. Picot, J. Ben-eveniste, 2012. Error Characterization of altimetry measurements at Climate Scales. Oral presentation at OSTST meeting, Venice, Italy, 27-28 September 2012. Available at: [http://www.aviso.altimetry.fr/fileadmin/documents/OSTST/2012/oral/02\\_friday\\_28/04\\_errors\\_uncertainties\\_I/03\\_EU1\\_Ablain.pdf](http://www.aviso.altimetry.fr/fileadmin/documents/OSTST/2012/oral/02_friday_28/04_errors_uncertainties_I/03_EU1_Ablain.pdf)
- [5] AVISO and PODAAC User Handbook. IGDR and GDR Jason-1 Products. Edition 4.1, October 2008. SMM-MU-M5-OP-13184-CN (AVISO), JPL D-21352 (PODAAC). Available at [http://www.aviso.oceanobs.com/fileadmin/documents/data/tools/hdbk\\_j1\\_gdr.pdf](http://www.aviso.oceanobs.com/fileadmin/documents/data/tools/hdbk_j1_gdr.pdf).
- [6] Beckley, B. D. , Zelensky, N. P. , Holmes, S. A. , Lemoine, F. G. , Ray, R. D. , Mitchum, G. T. , Desai, S. D. and Brown, S. T. (2010) Assessment of the Jason-2 Extension to the TOPEX/Poseidon, Jason-1 Sea-Surface Height Time Series for Global Mean Sea Level Monitoring, *Marine Geodesy*, 33:1, 447 - 471. Available at [http://pdfserve.informaworld.com/96442\\_\\_925511460.pdf](http://pdfserve.informaworld.com/96442__925511460.pdf)
- [7] Bertiger, Willy , Desai, Shailen D. , Dorsey, Angie , Haines, Bruce J. , Harvey, Nate , Kuang, Da. , Sibthorpe, Ant and Weiss, Jan P. (2010) Sub-Centimeter Precision Orbit Determination with GPS for Ocean Altimetry. *Marine Geodesy*, 33:1, 363 - 378. Available at [http://pdfserve.informaworld.com/858128\\_\\_925510150.pdf](http://pdfserve.informaworld.com/858128__925510150.pdf)
- [8] Bertiger, Willy , Desai, Shailen D. , Haines, Bruce J., R. DeCarvalho, and A. Dorsey (2010) Jason-2/OSTM Precision Orbit Determination with GPS Oral presentation at OSTST meeting, Lisbon, Portugal, Available at [http://www.aviso.oceanobs.com/fileadmin/documents/OSTST/2010/oral/19\\_Tuesday/bertiger.pdf](http://www.aviso.oceanobs.com/fileadmin/documents/OSTST/2010/oral/19_Tuesday/bertiger.pdf)
- [9] E. Bronner and G. Dibarboure, May 24th, 2012: Technical Note about the Jason-1 Geodetic Mission. SALP-NT-MA-EA-16267-CNv1.0. Available at: [http://www.aviso.oceanobs.com/fileadmin/documents/data/duacs/Technical\\_Note\\_J1\\_Geodetic\\_Mission.pdf](http://www.aviso.oceanobs.com/fileadmin/documents/data/duacs/Technical_Note_J1_Geodetic_Mission.pdf)
- [10] Bond, N. A., M. F. Cronin, H. Freeland, and N. Mantua (2015), Causes and impacts of the 2014 warm anomaly in the NE Pacific. *Geophys. Res. Lett.*, 42, 3414-3420. doi: 10.1002/2015GL063306.
- [11] Boening, C., J. K. Willis, F. W. Landerer, R. S. Nerem, and J. Fasullo (2012), The 2011 La Nina: So Strong, the Oceans Fell, *Geophys. Res. Lett.*, doi:10.1029/2012GL053055, in press.
- [12] Boy, François and Jean-Damien Desjonqueres. 2010. Note technique datation de l'instant de reflexion des échos altimètres pour POSEIDON2 et POSEIDON3 Reference: TP3-JPOS3-NT-1616-CNES
- [13] Brown G.S., "The average impulse response of a rough surface and its application", *IEEE Transactions on Antenna and Propagation*, Vol. AP 25, N1, pp. 67-74, Jan. 1977.
- [14] Brown S., S. Desai, and W. Lu "Initial on-orbit performance assessment of the advanced microwave radiometer and performance of JMR GDR-C", Oral presentation at OSTST meeting, Nice, France, 9-12 november 2008. Available at [http://www.aviso.oceanobs.com/fileadmin/documents/OSTST/2008/oral/brown\\_calval.pdf](http://www.aviso.oceanobs.com/fileadmin/documents/OSTST/2008/oral/brown_calval.pdf)
- [15] Brown, S., S. Desai, W. Lu, and A. Sibthorpe. 2009. Performance Assessment of the Advanced Microwave Radiometer after 1 Year in Orbit. Oral presentation at OSTST meeting, Seattle, USA. Available at: <http://www.aviso.oceanobs.com/fileadmin/documents/OSTST/2009/oral/Brown.pdf>
- [16] S. Brown. 2010. A Novel Near-Land Radiometer Wet Path-Delay Retrieval Algorithm: Application to the Jason-2/OSTM Advanced Microwave radiometer. *IEEE TGRS* vol. 48 n°4. Available at [ftp://podaac.jpl.nasa.gov/allData/ostm/preview/L2/AMR/docs/Brown\\_TGARS\\_2010.pdf](ftp://podaac.jpl.nasa.gov/allData/ostm/preview/L2/AMR/docs/Brown_TGARS_2010.pdf)
- [17] Cerri, L. , Berthias, J. P. , Bertiger, W. I. , Haines, B. J. , Lemoine, F. G. , Mercier, F. ,



- Ries, J. C. , Willis, P. , Zelensky, N. P. and Ziebart, M. (2010) Precision Orbit Determination Standards for the Jason Series of Altimeter Missions, *Marine Geodesy*, 33:1, 379 - 418. Available at [http://pdfserve.informaworld.com/816985\\_925509111.pdf](http://pdfserve.informaworld.com/816985_925509111.pdf)
- [18] Cerri, L., A. Couhert, S. Houry, F. Mercier. 2011. Improving the long-term stability of the GDR orbit solutions. Oral presentation at OSTST meeting, San Diego, USA. Available at [http://www.aviso.oceanobs.com/fileadmin/documents/OSTST/2011/oral/02\\_Thursday/Splinter3POD/05\\_Cerri.pdf](http://www.aviso.oceanobs.com/fileadmin/documents/OSTST/2011/oral/02_Thursday/Splinter3POD/05_Cerri.pdf).
- [19] Chambers, D., P., J. Ries, T. Urban, and S. Hayes. 2002. Results of global intercomparison between TOPEX and Jason measurements and models. Paper presented at the Jason-1 and TOPEX/Poseidon Science Working Team Meeting, Biarritz (France), 10-12 June.
- [20] Collard, F. (2005). Algorithmes de vent et période moyenne des vagues JASON à base de réseaux de neurons. BO-021-CLS-0407-RF. Boost Technologies.
- [21] Commien, L., S. Philipps, M. Ablain and N. Picot. 2009. SSALTO CALVAL Performance assessment Jason-1 GDR "C"/GDR "b". Poster presented at OSTST meeting, Seattle, USA. Available at: <http://www.aviso.oceanobs.com/fileadmin/documents/OSTST/2009/poster/commien.pdf>
- [22] Couhert, A., L. Cerri, F. Mercier, S. Houry. 2010. Status of Jason-1 and Jason-2 GDR orbits. Talk presented at OSTST meeting, Lisbon, Portugal. Available at: <http://www.aviso.oceanobs.com/fileadmin/documents/OSTST/2010/oral/couhert.pdf>
- [23] DeCarvalho, R., S. Brown, B. Haines and S. Desai. 2009. Global cross calibration and validation of the Jason-1 and Jason-2/OSTM data products. Oral presentation at OSTST meeting, Seattle, USA. Available at: <http://www.aviso.oceanobs.com/fileadmin/documents/OSTST/2009/oral/deCarvalho.pdf>
- [24] Desjonquères, J.-D., G. Carayon, J.-L. Courriere, and N. Steunou "POSEIDON-2 In-Flight results", Oral presentation at OSTST meeting, Nice, France, 9-12 november 2008.
- [25] Desjonquères, J. D. , Carayon, G. , Steunou, N. and Lambin, J. (2010) Poseidon-3 Radar Altimeter: New Modes and In-Flight Performances, *Marine Geodesy*, 33:1, 53 - 79. Available at [http://pdfserve.informaworld.com/542982\\_925503482.pdf](http://pdfserve.informaworld.com/542982_925503482.pdf)
- [26] Dettmering, Denise and Bosch, Wolfgang (2010) Global Calibration of Jason-2 by Multi-Mission Crossover Analysis, *Marine Geodesy*, 33:1, 150 - 161. Available at [http://pdfserve.informaworld.com/315039\\_925510361.pdf](http://pdfserve.informaworld.com/315039_925510361.pdf)
- [27] Dibarboure, G., F. Boy, J. D. Desjonqueres, S. Labroue, Y. Lasne, N. Picot, J. C. Poisson, and P. Thibaut, 2014: Investigating short-wavelength correlated errors on low-resolution mode altimetry. *J. Atmos. Oceanic Technol.*, **31**, 1337-1362, doi:[10.1175/JTECH-D-13-00081.1](https://doi.org/10.1175/JTECH-D-13-00081.1)
- [28] Dorandeu, J., M. Ablain, Y. Faugère, F. Mertz, 2004 : Jason-1 global statistical evaluation and performance assessment. Calibration and cross-calibration results. *Marine Geodesy* 27: 345-372.
- [29] Dufau, C., M. Orszynowicz, G. Dibarboure, R. Morrow, and P.-Y. Le Traon (2016), Mesoscale resolution capability of altimetry: Present and future, *J. Geophys. Res. Oceans*, 121, doi:10.1002/2015JC010904
- [30] Faugère, Y. et al. 2009. The SLOOP project: preparing the next generation of altimetry products for open ocean. Poster presented at OSTST meeting, Seattle, USA. Available at: <http://www.aviso.oceanobs.com/fileadmin/documents/OSTST/2009/poster/Faugere2.pdf>
- [31] Faugère, Y. et al. 2010. CROSS-CALIBRATION between ENVISAT and JASON-1/2. Oral presentation at OSTST meeting, Lisbon, Portugal. Available at: [http://www.aviso.oceanobs.com/fileadmin/documents/OSTST/2010/oral/19\\_Tuesday/Tuesday\\_afternoon/faugere.pdf](http://www.aviso.oceanobs.com/fileadmin/documents/OSTST/2010/oral/19_Tuesday/Tuesday_afternoon/faugere.pdf)
- [32] John T. Fasullo , C. Boening, F. W. Landerer, R. S. Nerem (2013), Australia's Unique Influence on Global Sea Level in 2010-2011, doi:10.1002/grl.50834, in press.
- [33] M. Guibbaud. A. Ollivier. Envisat RA2/MWR ocean data validation and cross calibration activities (Yearly report 2014). Reference: CLS.DOS/NT/14-253. Nomenclature: SALP-RP-MA-EA-22396-CLS.
- [34] Goussier, J., Vandemark, D., Bailey, S., Chapron, B., Gommenginger, G.P., Challenor, P.G. and Srokosz, M.A., 2002: A two-parameter wind speed algorithm for Ku-band altimeters, *Journal of Atmospheric and Oceanic Technology*. 19(12) 2030-2048.
- [35] Hernandez, F. and P. Schaeffer, 2000: Altimetric Mean Sea Surfaces and Gravity Anomaly maps inter-comparisons. AVI-NT-011-5242-CLS, 48 pp. CLS Ramonville St Agne.
- [36] Huffman, G. and D.T. Bolvin, 2009: TRMM and Other Data Precipitation Data Set Docu-



- mentation. Available at [ftp://precip.gsfc.nasa.gov/pub/trmmdocs/3B42\\_3B43\\_doc.pdf](ftp://precip.gsfc.nasa.gov/pub/trmmdocs/3B42_3B43_doc.pdf)
- [37] Imel, D.A. 1994. Evaluation of the TOPEX/POSEIDON dual-frequency ionospheric correction. *J. Geophys. Res.*, 99, 24,895-24,906.
- [38] Legeais J.F. and Ablain M., 2013: Validation of altimetric data by comparison with in-situ T/S Argo profiles (Annual Report 2013) [SALP-RP-MA-EA-22281-CLS, CLS.DOS/NT/13-256]
- [39] Legeais J.-F., P. Prandi, M. Ablain and S. Guinehut: Analyses of altimetry errors using Argo and GRACE data. *Ocean Science Discussion*, doi:10.5194/os-2015-111, in review, 2016.
- [40] Lemoine, F.G., Zelensky N.P., Chinn, D.S., et al. (2010), Towards development of a consistent orbit series for TOPEX, Jason-1, and Jason-2 *Adv. Space Res.*, 46(12), 1513-1540, doi: 10.1016/j.asr.2010.05.007 (updated).
- [41] Lemoine, F., N.P. Zelensky, S. Melachroinos, D.S. Chinn, B.D. Beckley, D.D. Rowlands, and S.B. Luthcke. 2011. GSFC OSTM (Jason-2), Jason-1 & TOPEX POD Update. Oral presentation at OSTST meeting, San Diego, USA. Available at [http://www.aviso.oceanobs.com/fileadmin/documents/OSTST/2011/oral/02Thursday/SplinterPOD/03Lemoine\\_etal\\_SWT2011\\_v01.pdf](http://www.aviso.oceanobs.com/fileadmin/documents/OSTST/2011/oral/02Thursday/SplinterPOD/03Lemoine_etal_SWT2011_v01.pdf).
- [42] Lemoine F., N.P. Zelensky, D.S. Chinn, B.D. Beckley, D.E. Pavlis, J. Wimert, O. Borydugov. 2014 : New GSC POD Standards for TOPEX/Poseidon, Jason-1, Jason-2 (OSTM). Oral presentation at OSTST meeting, Konstanz, Germany. Available at <http://www.aviso.altimetry.fr/fr/coin-utilisateur/equipes-scientifiques/sci-teams.html>.
- [43] Le Traon, P.-Y., J. Stum, J. Dorandeu, P. Gaspar, and P. Vincent, 1994: Global statistical analysis of TOPEX and POSEIDON data. *J. Geophys. Res.*, 99, 24619-24631.
- [44] Moyard J., E. Jalabert, A. Couhert, S. Rios-Bergantinos, F. Mercier, S. Houry. 2014 : Jason-2 POD status. Oral presentation at OSTST meeting, Konstanz, Germany. Available at <http://www.aviso.altimetry.fr/fr/coin-utilisateur/equipes-scientifiques/sci-teams.html>.
- [45] Moreau, T., P. Thibaut, 2009. Etude dépointage Poseidon-3: optimisation de l'angle d'ouverture d'antenne. CLS-DOS-NT-09-028. 15 pp, CLS Ramonville St. Agne.
- [46] Obligis, E., L. Eymard, M. Ablain, B. Picard, J.F. Legeais, Y. Faugere and N. Picot, 2010. The wet tropospheric correction for altimetry missions: A mean sea level issue. Oral presentation at OSTST meeting, Lisbon, Portugal. Available at [http://www.aviso.oceanobs.com/fileadmin/documents/OSTST/2010/oral/19\\_Tuesday/OBLIGIS.pdf](http://www.aviso.oceanobs.com/fileadmin/documents/OSTST/2010/oral/19_Tuesday/OBLIGIS.pdf).
- [47] Ollivier A., Faugere Y., P. Thibaut, G. Dibarboure, and J.-C. Poisson, 2008: Investigation on the high frequency content of Jason-1 and Jason-2. CLS.DOS/NT/09-027
- [48] Ollivier A., A. Couhert, V. Pignot, C. Renaudie, S. Phillips, N. Picot, 2014 : Assessment of orbit quality through the SSH calculation towards GDR-E standards. Oral presentation at OSTST meeting, Constance, Germany. Available at <http://www.aviso.altimetry.fr/fr/coin-utilisateur/equipes-scientifiques/sci-teams.html>
- [49] Ollivier A., S. Philipps, M. Ablain, A. Edwell, L. Cerri, N. Picot, 2013 : Assessment of Orbit Quality through the Sea Surface Height calculation, New insight in resolving long term and inter-annual signal for climate studies. Oral presentation at OSTST meeting, Boulder, USA. Available at <http://www.aviso.altimetry.fr/fr/coin-utilisateur/equipes-scientifiques/sci-teams.html>
- [50] Ollivier A., Dibarboure G., Picard B., Ablain M., OSTST2014, Konstanz - Germany, "Spectral analysis of altimetric signal and errors Towards a spectral error budget of Nadir Altimetric missions" [http://meetings.aviso.altimetry.fr/fileadmin/user\\_upload/tx\\_ausyclsseminar/files/30Ball0900-2\\_Pres\\_OSTST2014\\_J2\\_ErrorBugdet\\_Spectra\\_Ollivier.pdf](http://meetings.aviso.altimetry.fr/fileadmin/user_upload/tx_ausyclsseminar/files/30Ball0900-2_Pres_OSTST2014_J2_ErrorBugdet_Spectra_Ollivier.pdf)
- [51] Otten M., C. Flohrer, T. Springer, and W. Enderle. 2011. Generating precise and homogeneous orbits for Jason-1 and Jason-2. Oral presentation at OSTST meeting, San Diego, USA. Available at [http://www.aviso.oceanobs.com/fileadmin/documents/OSTST/2011/oral/03\\_Friday/Splinter6POD/01\\_Otten.pdf](http://www.aviso.oceanobs.com/fileadmin/documents/OSTST/2011/oral/03_Friday/Splinter6POD/01_Otten.pdf).
- [52] Peltier, 2004, Global Glacial Isostasy And The Surface of The Ice-Age Earth: The ICE-5G (VM2) Model and GRACE. *Annual Review of Earth and Planetary Sciences*, May 2004, Vol. 32, Pages 111-149, doi: 10.1146/annurev.earth.32.082503.144359
- [53] Picot, N., P. Thibaut, N. Tran, S. Philipps, J.C. Poisson, E. Bronner, C. Garcia and many others. 2011. Jason-2 GDR-D standards. Oral presentation at OSTST meeting, San Diego, USA. Available at [http://www.aviso.oceanobs.com/fileadmin/documents/OSTST/2011/oral/02\\_Thursday/Splinter5IP/05NPicot\\_et\\_al\\_OSTST\\_2011\\_J2-GDRD-Standards.pdf](http://www.aviso.oceanobs.com/fileadmin/documents/OSTST/2011/oral/02_Thursday/Splinter5IP/05NPicot_et_al_OSTST_2011_J2-GDRD-Standards.pdf).
- [54] Picot, N., S. Desai, E. Leuliette, R. Scharroo. 2016. Cross calibration and validation of Jason-2



and Jason-3. Oral presentation at OSTST meeting, La Rochelle, FR. Available at <http://www.aviso.oceanobs.com/>

[55] Prandi P., Valladeau G., 2015: Validation of altimeter data by comparison with tide gauge measurements for TOPEX/Poseidon, Jason-1, Jason-2 and Envisat (Annual report 2015).

[SALP-RP-MA-EA-22956-CLS, CLS.DOS/NT/15-062].

[56] Prandi P., Legeais J.F. and Ablain M., 2015: Validation of altimetric data by comparison with in-situ T/S Argo profiles (Annual Report 2015) [SALP-RP-MA-EA-22966-CLS, CLS.DOS/NT/15-068]

[57] Prandi P., Debout V.: Validation of altimeter data by comparison with tide gauges measurements: yearly report 2016 for TOPEX/Poseidon, Jason-1, Jason-2, ERS-2, Envisat and SARAL/AltiKa. SALP-RP-MA-EA-23082-CLS.

[58] Renaudie C., S. Philipps, 2014: Comparison of the latest GSFC SLR/DORIS std1204 orbits with current orbits for TP,J1 and J2. CLS Ramonville St Agne.

[59] Roinard, H., Philipps S., Jason-2 reprocessing impact on ocean data (cycles 001 to 020). Comparison of Jason-2 Gdr-D with Gdr-T, as well as with Jason-1 Gdr-C. SALP-RP-MA-EA-22118-CLS. CLS.DOS/NT/12.138. Available at [ftp://avisoftp.cnes.fr/AVISO/pub/jason-2/documentation/gdr\\_d\\_calval\\_report/JA2\\_GDR\\_D\\_validation\\_report\\_cycles1to20\\_V1\\_1.pdf](ftp://avisoftp.cnes.fr/AVISO/pub/jason-2/documentation/gdr_d_calval_report/JA2_GDR_D_validation_report_cycles1to20_V1_1.pdf)

[60] Roinard, H., S. Philipps. Jason-2 reprocessing impact on ocean data (cycles 001 to 145). Comparison of Jason-2 Gdr-D with Gdr-T, as well as with Jason-1 Gdr-C and Envisat Gdr v2.1. SALP-RP-MA-EA-22140-CLS. CLS.DOS/NT/12.222.

[61] Schaeffer, P., Y. Faugere, J.-F. Legeais, A. Ollivier, T. Guinle, and N. Picot (2012). The CNES CLS11 Global Mean Sea Surface Computed from 16 Years of Satellite Altimeter Data. *Marine Geodesy* 35: sup1, 3-19. Available at <http://www.tandfonline.com/doi/abs/10.1080/01490419.2012.718231>

[62] Scharroo, R., J. Lillibridge, and W.H.F. Smith, 2004: Cross-calibration and long-term monitoring of the Microwave Radiometers of ERS, Topex, GFO, Jason-1 and Envisat. *Marine Geodesy*, 97.

[63] Thibaut, P. O.Z. Zanif, J.P. Dumont, J. Dorandeu, N. Picot, and P. Vincent, 2002. Data editing: The MQE criterion. Paper presented at the Jason-1 and TOPEX/Poseidon Science Working Team Meeting, New-Orleans (USA), 21-23 October.

[64] Tran, N., Labroue, S., Philipps, S., Bronner, E. and Picot, N. (2010) Overview and Update of the Sea State Bias Corrections for the Jason-2, Jason-1 and TOPEX Missions, *Marine Geodesy*, 33:1, 348 - 362. Available at [http://pdfserve.informaworld.com/804727\\_925502357.pdf](http://pdfserve.informaworld.com/804727_925502357.pdf)

[65] Valladeau, G., J.F. Legeais, M. Ablain, S. Guinehut, and N. Picot, 2012: Comparing altimetry with tide gauges and Argo profiling floats for data quality assessment and Mean Sea Level studies. *Marine Geodesy* 2012, DOI: 10.1080/01490419.2012.718226.

[66] World Meteorological Organization, 2010: El Nino/ La Nina Update (30 March 2010). Available at [http://www.wmo.ch/pages/prog/wcp/wcasp/documents/El\\_Nino\\_Mar10\\_Eng.pdf](http://www.wmo.ch/pages/prog/wcp/wcasp/documents/El_Nino_Mar10_Eng.pdf).

[67] World Meteorological Organization, 2011: El Nino/ La Nina Update (25 January 2011). Available at [http://www.wmo.ch/pages/prog/wcp/wcasp/documents/El-Nino\\_Jan11\\_Eng.pdf](http://www.wmo.ch/pages/prog/wcp/wcasp/documents/El-Nino_Jan11_Eng.pdf).

[68] World Meteorological Organization, 2015: El Nino/ La Nina Update (16 November 2015). Available at [http://www.wmo.int/pages/prog/wcp/wcasp/documents/WMO\\_ENSO\\_Nov15\\_Eng.pdf](http://www.wmo.int/pages/prog/wcp/wcasp/documents/WMO_ENSO_Nov15_Eng.pdf)

[69] Edward D. Zaron, Robert deCarvalho, 2016. Identification and Reduction of Retracker-Related Noise in Altimeter-Derived Sea Surface Height Measurements. *Journal of Atmospheric and Oceanic Technology*, p201-210, 10.1175/JTECH-D-15-0164.1 [doi]

[70] Zlotnicky, V. 1994. Correlated environmental corrections in TOPEX/POSEIDON, with a note on ionospheric accuracy. *J. Geophys. Res.*, 99, 24,907-24,914

[71] Zawadzki L., Taburet N.: Validation of altimeter data by comparison with in-situ T/S Argo profiles (Annual Report 2016). SALP-RP-MA-EA-22966-CLS.

[72] Zawadzki, L., M. Ablain, A. Cazenave, B. Meyssignac. 2014. Confidence envelop of the Global MSL time-series deduced from Jason-1 and Jason-2 altimetric missions. Poster presentation at OSTST meeting, Constance, Germany, 28-31 October 2014, Available at [http://meetings.aviso.altimetry.fr/fileadmin/user\\_upload/tx\\_ausyclsseminar/files/Poster\\_OSTST14\\_GMSLUncertainty.pdf](http://meetings.aviso.altimetry.fr/fileadmin/user_upload/tx_ausyclsseminar/files/Poster_OSTST14_GMSLUncertainty.pdf)



SALP-RP-MA-EA-  
23060-CLS

V 1.2      Mar. 29, 17